AD-A162 432 RESEARCH ON AERO-THERMODYNAMIC DISTORTION INDUCED 1/1
STRUCTURAL DYNAMIC RESP..(U) PURDUE UNIV LAFAYETTE IN
SCHOOL OF MECHANICAL ENGINEERING S FLEETER JUN 84
UNCLASSIFIED ME-TSPC-TR-84-03 AFOSR-TR-85-1060 F/G 21/5 NL

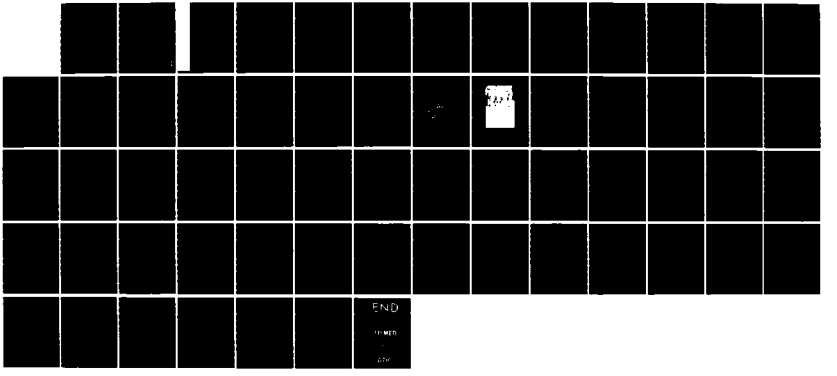

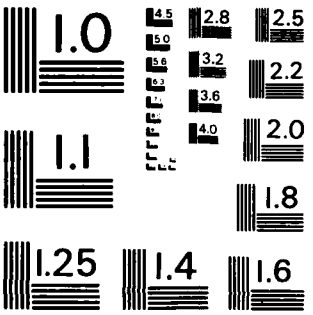

UNCLASSIFIED

AD-A162 432

(2)

REPORT DOCUMENTATION PAGE

1a. REPORT SECURITY CLASSIFICATION: Unclassified	1b. RESTRICTIVE MARKINGS
2a. SECURITY CLASSIFICATION AUTHORITY	3. DISTRIBUTION/AVAILABILITY OF REPORT: **Approved for public release, distribution unlimited**
2b. DECLASSIFICATION/DOWNGRADING SCHEDULE	
4. PERFORMING ORGANIZATION REPORT NUMBER(S)	5. MONITORING ORGANIZATION REPORT NUMBER(S): **AFOSR-TR- 85-1060**
6a. NAME OF PERFORMING ORGANIZATION: PURDUE UNIVERSITY	6b. OFFICE SYMBOL (If applicable)
7a. NAME OF MONITORING ORGANIZATION: AFOSR/NA	
6c. ADDRESS (City, State and ZIP Code): THERMAL SCIENCES AND PROPULSION CENTER, SCHOOL OF MECHANICAL ENGINEERING, WEST LAFAYETTE, IN 47907	7b. ADDRESS (City, State and ZIP Code): BOLLING AFB, DC 20332-6448
8a. NAME OF FUNDING/SPONSORING ORGANIZATION: AIR FORCE FFICE OF SCIENTIFIC RESEARCH	8b. OFFICE SYMBOL (If applicable): AFOSR/NA
9. PROCUREMENT INSTRUMENT IDENTIFICATION NUMBER: F49620-83-K-0029	
8c. ADDRESS (City, State and ZIP Code): OLLING AFB, DC 20332-6448	10. SOURCE OF FUNDING NOS.

PROGRAM ELEMENT NO.	PROJECT NO.	TASK NO.	WORK UNIT NO.
61102F	2307	A4	

11. TITLE (Include Security Classification): RESEARCH ON AERO-THERMODYNAMIC DISTORTION INDUCED STRUCTURAL DYNAMIC RESPONSE OF MULTI-STAGE COMPRESSOR BLADING (UNCLASSIFIED)

12. PERSONAL AUTHOR(S): S. FLEETER

13a. TYPE OF REPORT	13b. TIME COVERED	14. DATE OF REPORT (Yr., Mo., Day)	15. PAGE COUNT
ANNUAL	FROM 16 Apr 83 TO 15 Apr 84	June 84	52

16. SUPPLEMENTARY NOTATION

17. COSATI CODES			18. SUBJECT TERMS (Continue on reverse if necessary and identify by block number)
FIELD	GROUP	SUB GR	
			TURBOMACHINERY STRUCTURAL DYNAMIC RESPONSE UNSTEADY AERODYNAMICS AEROTHERMODYNAMIC DISTORTION

19. ABSTRACT (Continue on reverse if necessary and identify by block number)

The overall objective of this research program is to quantitatively investigate the fundamental phenomena relevant to aerothermodynamic distortion induced structural dynamic blade response in multi-stage gas turbine fans and compressors.

This report summarizes the progress and results obtained during the period April 16, 1983 to April 15, 1984. These include; the calibration of stator vanes instrumented with dynamic pressure transducers; the completion and verification of the steady and dynamic data acquisition and analysis procedures; the check-out and initial experimental study of the first stage vane row unsteady aerodynamics; the initiation of the development of the dynamic instrumentation and calibration procedures for the roter studies; and the completion of the structural dynamics portion of the coupled mode blade vibration energy balance structural dynamics math model.

20. DISTRIBUTION/AVAILABILITY OF ABSTRACT	21. ABSTRACT SECURITY CLASSIFICATION
UNCLASSIFIED-UNLIMITED ☒ SAME AS RPT ☐ DTIC USERS ☐	Unclassified

22a. NAME OF RESPONSIBLE INDIVIDUAL	22b. TELEPHONE NUMBER (Include Area Code)	22c. OFFICE SYMBOL
JAMES D WILSON	(202) 767-4935	AFOSR/NA

DD FORM 1473, 83 APR — EDITION OF 1 JAN 73 IS OBSOLETE

SECURITY CLASSIFICATION OF THIS PAGE

AD-A162 432

AFOSR-TR- 85-1060

Report ME-TSPC-TR-84-03
June 1984

Annual Summary Report
Contract F49620-83-K-0029

Research on Aero-Thermodynamic Distortion Induced Structural Dynamic Response of Multi-Stage Compressor Blading

Sanford Fleeter

Thermal Science and Propulsion Center
School of Mechanical Engineering
Purdue University
West Lafayette, Indiana 47907

Prepared for
Directorate of Aerospace Sciences
Air Force Office of Scientific Research

Report ME-TSPC-TR-84-03

ANNUAL SUMMARY REPORT
April 1983-1984

CONTRACT F49620-83-K-0029

RESEARCH ON AERO-THERMODYNAMIC DISTORTION INDUCED STRUCTURAL DYNAMIC RESPONSE OF MULTI-STAGE COMPRESSOR BLADING

SANFORD FLEETER

June 1984

Thermal Sciences and Propulsion Center
School of Mechanical Engineering
Purdue University
West Lafayette, Indiana 47907

Prepared for

Directorate of Aerospace Sciences
Air Force Office of Scientific Research

ABSTRACT

The structural dynamic response of turbomachinery components to aero-thermodynamic distortion induced excitations is an item of major concern in the design of advanced gas turbine engines. The rotor speeds at which these resonant forced responses occur can be predicted with Campbell diagrams. However, due to the inadequacies of the existing time-variant aerodynamic models, no accurate prediction can currently be made for the amplitude of the resulting stresses.

The overall objective of this research program is to quantitatively investigate the fundamental phenomena relevant to aero-thermodynamic distortion induced structural dynamic blade response in multi-stage gas turbine fans and compressors. Unique unsteady aerodynamic data will be obtained to validate and indicate necessary refinements to state-of-the-art analyses and to direct the modeling of new analyses. Also, for the first time, a first principles capability to predict the vibrational response amplitude of blading due to aerodynamic excitations will be developed.

This report summarizes the progress and results obtained during the period April 16, 1983 to April 15, 1984. These include: the calibration of stator vanes instrumented with dynamic pressure transducers; the completion and verification of the steady and dynamic data acquisition and analysis procedures; the check-out and initial experimental study of the first stage vane row unsteady aerodynamics; the initiation of the development of the dynamic instrumentation and calibration procedures for the rotor studies; and the completion of the structural dynamics portion of the coupled mode blade vibration energy balance structural dynamics math model.

TABLE OF CONTENTS

I. INTRODUCTION

The structural dynamic response of fan, compressor, and turbine blading to aero-thermodynamic distortion induced excitations is an item of rapidly increasing concern to designers and manufacturers of gas turbine engines for advanced technology applications. Destructive aerodynamic forced responses of gas turbine engine blading have been generated by a wide variety of aero-thermodynamic distortion sources. These include: blade wakes; multi-staging interaction effects; large angle of attack or yaw; engine exhaust recirculation; cross-flow at the inlet; pressure variations on the engine due to external aerodynamics; and armament firing. The following physical phenomena have been identified as being significant with regard to aero-thermodynamic distortion induced structural dynamic responses of fan and compressor blading.

* Resonance
* Multi-stage interactions
* Stall
* Inlet gusts
* Time-varying inlet flows

* Flow separation

* Potential effects

* Turbulence

The first principles prediction of the structural dynamic response associated with all of the above physical phenomena is identical and involves the following elements. Spatially periodic variations in pressure, velocity, temperature, and flow direction of the exit flow field of an upstream element appear as temporally varying in a coordinate system fixed to the downstream row. As a result, individual airfoils are subject to a time-variant aerodynamic forcing function which can induce high level vibratory stresses.

The analysis of the aerodynamically forced response vibratory behavior of a blade or vane row requires a definition of the unsteady forcing function in terms of its harmonics. The time-variant aerodynamic response of the airfoil to each harmonic of this forcing function is then assumed to be comprised of two parts. One is due to the disturbance being swept past the non-responding fixed airfoils. The second arises when the airfoils respond to this disturbance. Mathematically these effects are modeled by two distinct analyses. A linearized small perturbation gust analysis is used to predict the time-variant aerodynamics of the fixed non-responding airfoils to each harmonic of the disturbance. A self-induced unsteady aerodynamic analysis

wherein the airfoils are assumed to be harmonically oscillating is then used to predict the additional aerodynamic effects due to the airfoil response. Superposition of these two effects can be performed only with knowledge of the modal pattern and amplitude of response of the blading because the magnitude of the pressure field resulting from the airfoil motion is dependent upon the amplitude of this motion. Thus a solution with key elements consisting of the gust analysis, a self-induced unsteady aerodynamic analysis, and an airfoil structural analysis is necessary to predict the total response of an airfoil subjected to an upstream generated spatially periodic disturbance.

The unsteady small perturbation gust and self-induced unsteady aerodynamic analyses are two-dimensional and, as such, are coupled to the airfoil structural analysis by means of a strip theory approximation. Thus, the airfoil is considered to consist of a series of individual and independent two-dimensional aerodynamic regions. The time-variant aerodynamic analyses are then applied to each such individual region, with the characteristic parameters including the Mach number, reduced frequency, stagger angle, and solidity, taken as the average value at the inlet boundary. It should be noted that there is no coupling between adjacent aerodynamic regions. Hence, aerodynamic forced vibrations involving spanwise variations in unsteady aerodynamics cannot be treated, i.e., if spanwise variations exist in the aerodynamic forcing function not caused by simple inlet spanwise variations in the Mach number, reduced frequency, stagger angle,

or solidity, such a strip theory design system is of no value. Some of the previously noted forced response sources may fit into this category, as for example, the case of rotor tip vortices generating a forced response in a downstream blade or vane row.

II. PROGRAM OBJECTIVES

Overall Objectives

The overall objective of this research program is to quantitatively investigate the fundamental phenomena relevant to distortion generated aero-thermodynamic induced structural dynamic effects in gas turbine engine blade rows. Unique unsteady aerodynamic data will be obtained on stationary and rotating blade rows to validate and indicate necessary refinements to current state-of-the-art analyses and to direct the modeling and development of new analyses. Also, for the first time, a first principles capability to predict the vibrational response amplitude of blading due to aerodynamic excitations based on an energy balance technique will be developed.

From first principles considerations, the relevant fundamental physical phenomena are identical for the various sources of aero-thermodynamic distortion. Hence, to accomplish this overall objective in a timely and efficient manner, while obtaining results of direct interest and significance to the gas turbine engine community, this proposed research program is concerned with the time-variant aerodynamics and structural dynamic response of multi-stage stationary and rotating blade rows, with the primary source of excitation initially being the wakes from upstream blade elements. The overall objective includes the following:

* The experimental determination of the fundamental time-variant gust aerodynamics associated with variations in incidence angle (loading), reduced frequency, solidity, and multi-stage effects on both stationary and rotating blade rows as well as the investigation of the validity of:
  * the two-dimensional linearity and superpositioning assumptions;
  * the small perturbation modeling concept;
* The development of a first principles state-of-the-art capability to predict the vibrational response amplitude of blading based on an energy balance technique, with key elements consisting of the following coupled existing analyses:
  * a flat plate cascade transverse gust analysis;
  * a flat plate cascade self-induced unsteady aerodynamics analysis;
  * an airfoil structural analysis;

* The development of a subsonic compressible unsteady aerodynamic cascade analysis.

Thus, this program is directed at providing fundamental time-variant aerodynamic data whic` will not only validate and indicate refinements to the current state-of-the-art two-dimensional gust analyses but will also address the validity of the most basic assumptions inherent in these analyses and in the structure of forced response design systems. In addition a state-of-the-art first prinicples predictive aerodynamically forced response analysis based on an energy balance technique will be developed.

Specific Objectives

The following were the specific objectives for this reporting period.

Stationary Vane Row Experiments

* Calibration of the stator vanes instrumented with Kulite dynamic pressure transducers
* Completion and verification of the steady and dynamic data acquisition and analysis procedures
* On-line check out of the data acquisition system

* Initiation of the acquisition and analysis of the first stage vane row time-variant aerodynamic data

Rotor Blade Studies

* Initiation of the development of the dynamic instrumentation and calibration procedures for the first stage rotor blade row

Analysis

* Parametric studies completed with the coupled mode blade vibration energy balance structural dynamics mathematical model

III. TECHNICAL APPROACH

The technical approach to achieve the overall program objectives requires that extensive, high-quality, detailed aerodynamic data be acquired from benchmark experiments which model the fundamental flow physics of aero-thermodynamic induced structural dynamic effects in gas turbine engines. These data must be analyzed and correlated with appropriate state-of-the-art analyses to ascertain their range of validity and/or to indicate necessary refinements. In addition, advanced mathematical models and techniques for the prediction of these phenomena will be developed and experimentally verified.

The approach to achieving these experimental objectives is to measure the time-variant pressure distribution in controlled benchmark experiments which model the fundamental flow physics and thereby identify and quantify the key unsteady aerodynamic parameters relevant to aero-thermodynamic distortion induced response of blading. In particular, this research program is aimed at measuring the fundamental unsteady gust aerodynamics associated with variations in incidence angle (loading), reduced frequency, solidity, multi-stage effects, as well as investigating the validity of the two-dimensional linearity and superpositioning assumptions and the applicability of the small perturbation modeling concept. This requires obtaining airfoil surface chordwise and spanwise unsteady pressure data on both stationary

and rotating blade rows as well as detailed inlet and exit plane flow surveys in a multi-stage axial flow compressor. These data will be correlated with state-of-the-art unsteady cascade transverse gust analyses and will be used to determine their range of validity and to direct the development of an advanced first principles forced vibration aerodynamic analysis which the designer can use with confidence. In addition, a unique first principles predictive aerodynamically forced response analysis will be developed based on an energy balance technique.

Facility

In the first stage of a multi-stage axial flow compressor the wakes from the upstream rotor blades are the source of the aerodynamically induced fluctuating surface pressures on the downstream stator vanes; i.e., the rotor blade wakes define the forcing function to the downstream stator vane row. In the aft stages of the compressor the wakes from all of the upstream blading, both rotors and stators, are the source of the aerodynamically induced fluctuating surface pressure distributions on the downstream stator vane and rotor blade rows. Hence, it is necessary to experimentally model all of the significant features which define this forcing function. These include the variation of incidence, the wave form, the velocity (pressure) variation, the various blade row interactions in a multi-stage machine, and the reduced frequency ($k = \omega C / 2V_{axial}$) which defines the order of magnitude of the unsteadiness. (Forced response problems in

turbomachines typically have first harmonic reduced frequency values varying from 0.2 to 8.0.) The above noted features can all be simulated in the Purdue University Multi-Stage Axial Flow Research Compressor.

Figure 1 presents a schematic of the overall facility, with the compressor test section shown in greater detail in Figures 2 and 3. The compressor is driven by a 15 HP DC electric motor with a speed range of 300 to 3000 RPM. The inlet section is located aft of the drive motor. In the exit of this section are located 38 variable geometry guide vanes which direct the flow into the test section. Three identical compressor stages are mounted in the test section, which has an annulus with constant hub (0.300 m) and tip (0.420 m) diameters. The exit flow from the test section is directed through a series of flow straighteners into a venturi meter which enables the mass flow rate to be determined. To throttle the compressor, an adjustable plate is located at the exit of the diffuser of the venturi.

Each of the three identical compressor stages consists of 43 rotor blades and 41 stator vanes. Hence, the interblade phase angle for these experiments is 17.56°. These free vortex design airfoils have a British C4 section profile, a chord of 30 mm, and a maximum thickness-to-chord ratio of 0.10. The overall airfoil and compressor characteristics are presented in Table I.

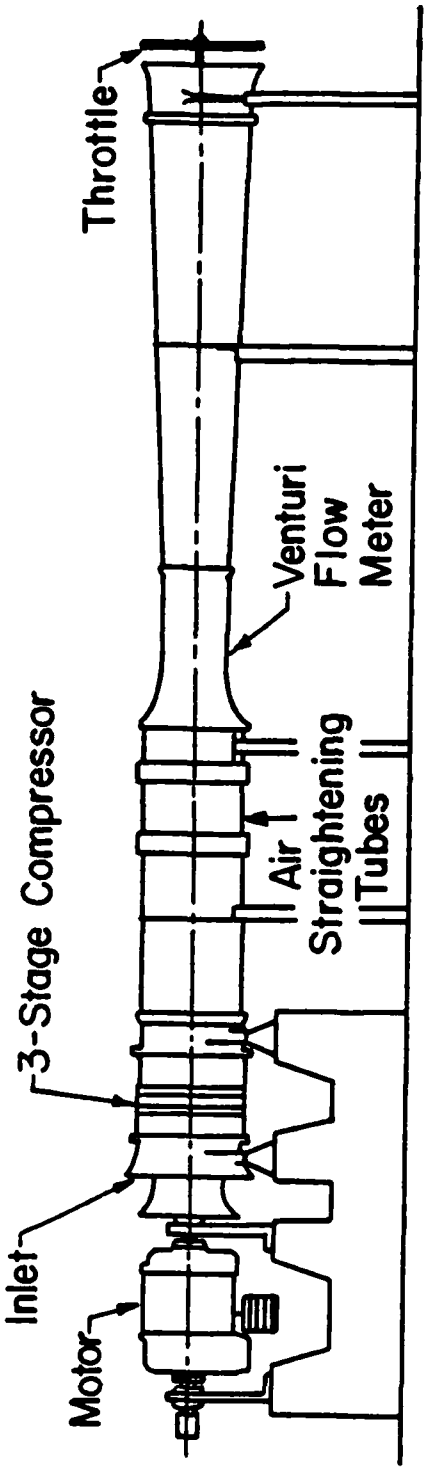

Figure 1. Schematic of overall facility

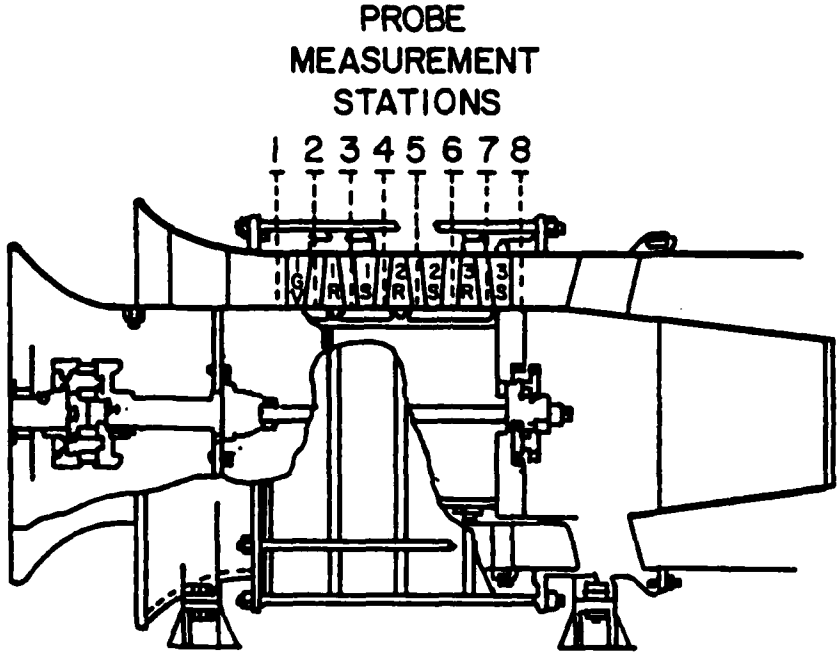

Figure 2. Schematic of compressor test section

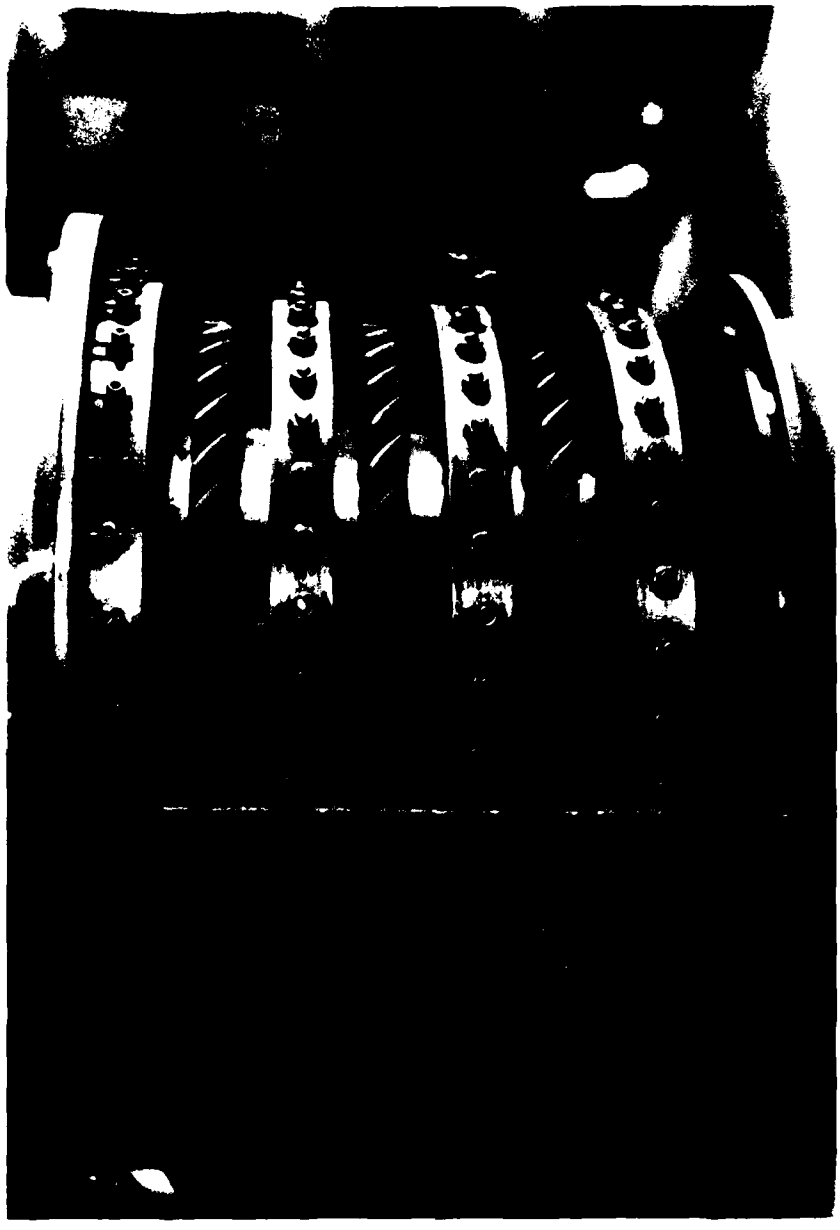

Figure 3. Close-up view of the blading of the Three-Stage Research Compressor

	Rotor	Stator
Type of Airfoil	C4	C4
Number of Blades	43	41
Chord, C(mm)	30	30
Solidity, C/S	1.14	1.09
Camber	27.95	27.70
Aspect Ratio	2.0	2.0
Thickness/Chord (%)	10	10
Flow Rate (kg/second)	2.66	
Rotor-Stator Axial Spacing (mm)	22.2	
Design Axial Velocity (meters/sec)	32.0	
Rotational Speed (RPM)	3000	
Number of Stages	3	
Stage Pressure Ratio	1.003	
Inlet Tip Diameter (mm)	420	
Hub/Tip Radius Ratio	0.714	
Stage Efficiency (%)	85	

TABLE I. AIRFOIL MEAN SECTION CHARACTERISTICS AND COMPRESSOR DESIGN POINT CONDITIONS

Conventional steady-state instrumentation is used to determine the flow properties in the compressor. The inlet temperature is measured by four equally spaced thermocouples at the inlet of the compressor. Casing static taps, equally spaced circumferentially, allow the measurement of the static pressure between each blade row. Traversing gear instrument stations provided between each blade row are used to measure the mean flow incidence angle on the first-stage stator vanes. A thermocouple and Kiel probe located downstream are used to measure the compressor exit temperature and total pressure, respectively. The mass flow is measured with the calibrated venturi meter located downstream of the compressor test section. A shaft mounted 60 tooth gear and a magnetic pickup provide the rotor speed.

IV. PROGRAM STATUS AND RESULTS

All of the previously noted specific objectives established for this reporting period have been successfully met.

Stationary Vane Row Experiments

The calibration, steady and dynamic data acquisition and analysis procedures, and the check-out of the data acquisition system have been completed. Also, the initial acquisition and analysis of the first stage vane row time-variant data has begun.

Initial Check-Out Experiment

In this initial first stage stator vane check-out study, the wakes from the first stage rotor blades are the source of the aerodynamically induced fluctuating surface pressure distributions, i.e., the rotor wakes define the forcing function to the first stage stator vanes, as schematically depicted in Figure 4.

The unsteady data of fundamental interest are the chordwise distribution of the complex time-variant pressure difference across the chordline of the first stage stator vane. This requires the measurement of the dynamic pressure distributions on the pressure and suction surfaces of the first stage stator vane

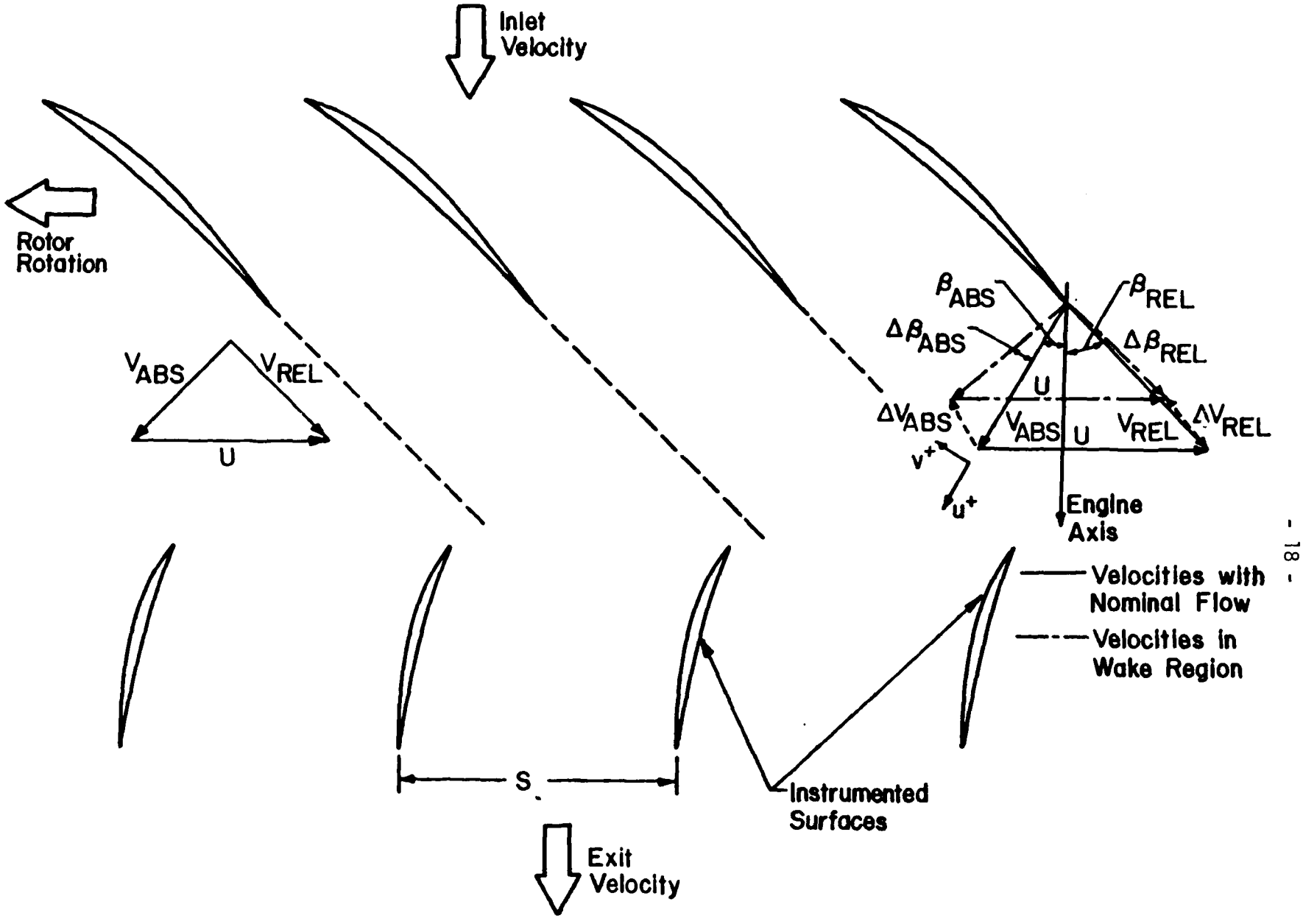

Figure 4. Schematic of flow field

at identical chordwise locations. These airfoil surface fluctuating pressure measurements are accomplished by instrumenting pairs of stator vanes with Kulite thin-line design dynamic pressure transducers.

To minimize any flow disturbances generated by the transducers, they were embedded in the airfoil and connected to the surface by a static pressure tap. The transducer lead wires were placed in milled slots and carried out through hollow trunnions. A similar installation was used for the transducers on the pressure surface at the same chord locations. Thus, in this initial check-out study, sets of two instrumented vanes were used, one with suction surface transducers and one with pressure surface transducers. These vanes were located such that a complete flow passage was instrumented. Conventional static pressure taps were also provided at the same locations. These static pressure taps provide the steady state aerodynamic load distribution on the airfoil.

Both steady-state and time-variant data are being acquired. Figure 5 presents a schematic of the complete data acquisition and analysis system which is centered on a PDP 11-23 computer.

The steady-state data of interest include: (1) the static pressures on the stator vane surfaces, accomplished with chordwise distributions of surface static pressure taps; (2) the pressures and temperatures throughout the compressor, thereby permitting the compressor operating map to be determined, as shown in

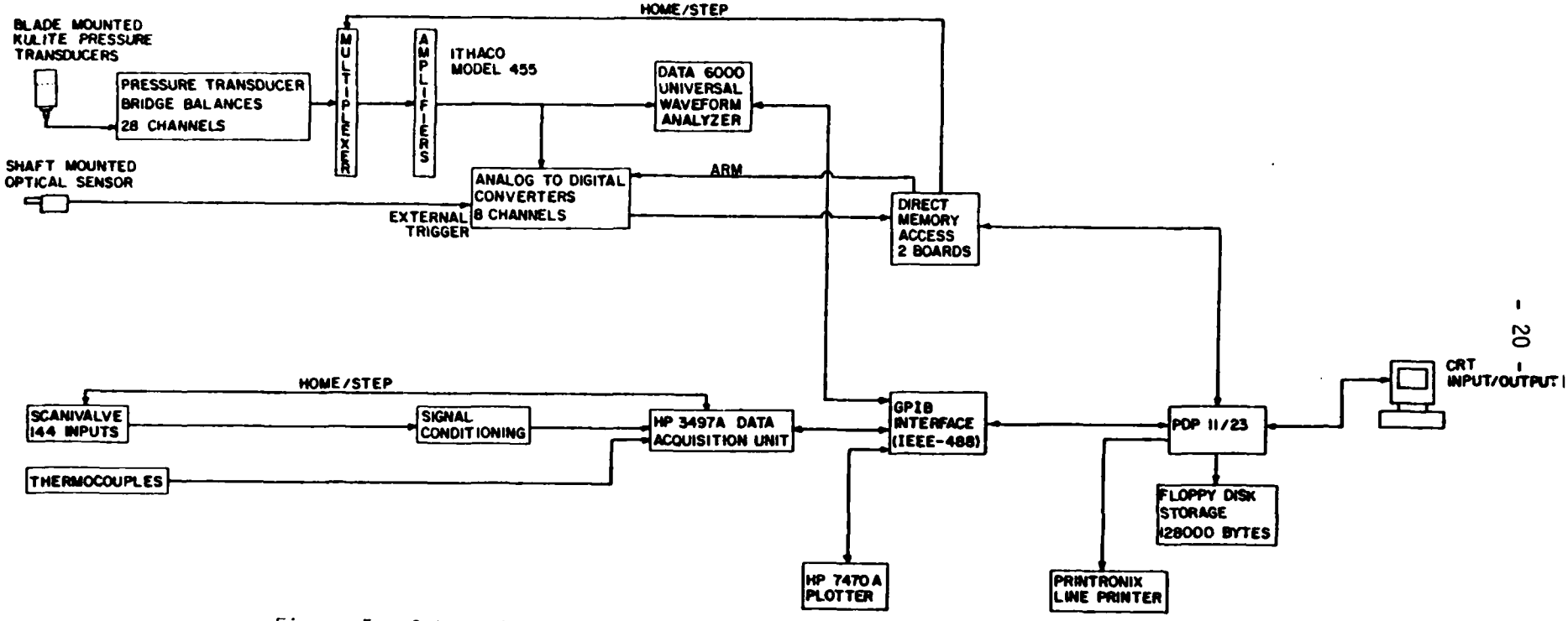

Figure 5. Schematic of online computer controlled data acquisition system

Figure 6. The compressor map is used to define the operating points, in terms of overall pressure ratio and corrected mass flow rate, at which the unsteady surface pressure measurements are obtained.

Steady-state data acquisition follows the standard evaluation procedure. At the selected corrected speed, the compressor is stabilized for approximately 10 minutes, after which the steady-state sequence is initiated. The data are then scanned, and the corrected mass flow, pressure ratio, and corrected speed determined.

The time-variant data acquisition and analysis technique used is based on a data averaging or signal enhancement concept. The key to such a technique is the ability to sample data at a preset time. In this investigation, the data of interest are being generated at the blade passing frequency. Hence, an optical encoder, delivering a square wave voltage signal with a duration in the microsecond range, was mounted on the rotor shaft and used as the time or data initiation reference to trigger the A-D multiplexer system. This system is capable of digitizing signals simultaneously at rates to 5 megahertz per channel, storing 2048 data points per channel.

In this initial check-out experiment, the effect of averaging the time-variant pressure signals from the blade mounted dynamic pressure transducers was considered. Figures 7 through 11 display the time-variant pressure signal from the 14.1% chord

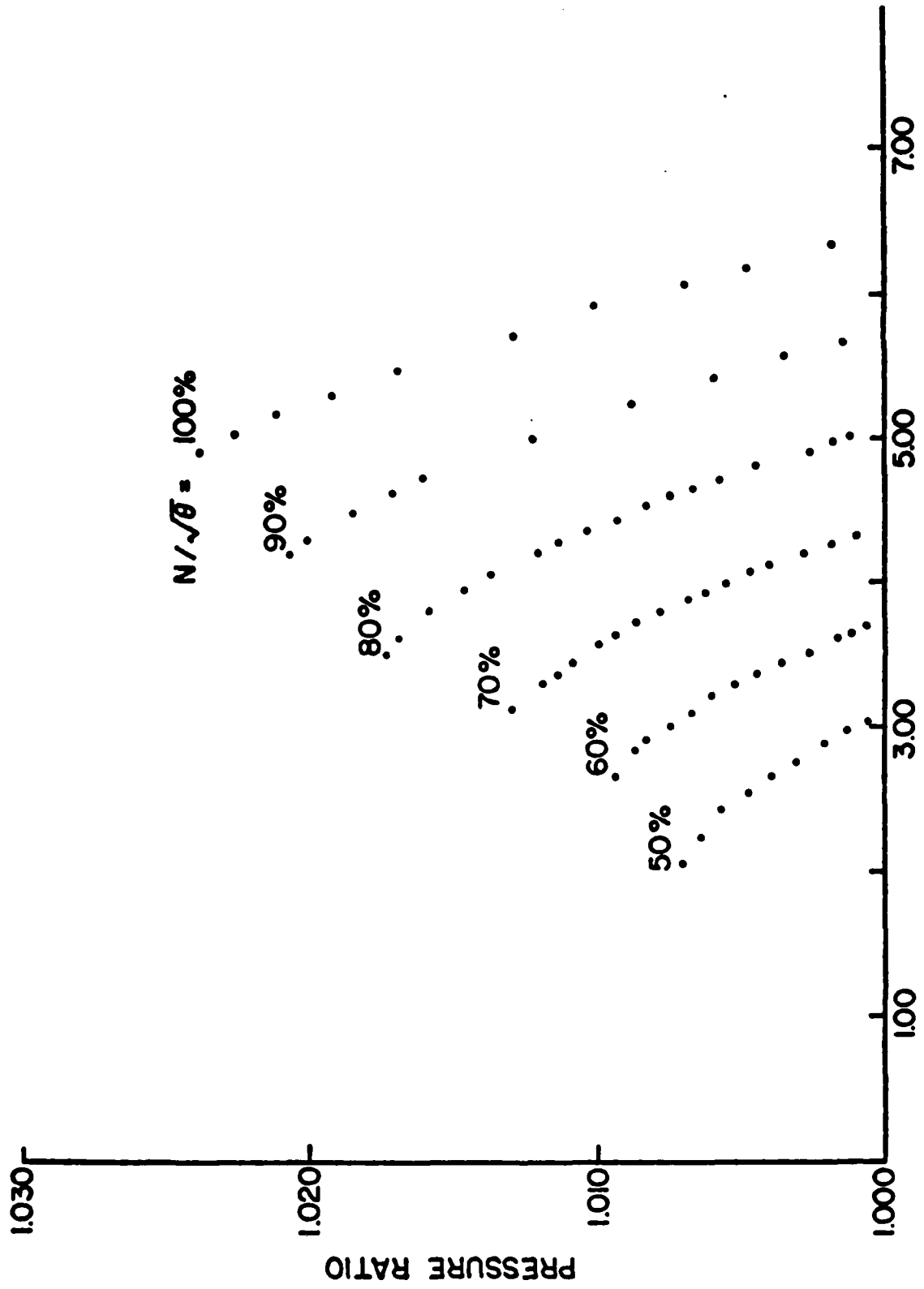

Figure 6. Overall compressor performance map

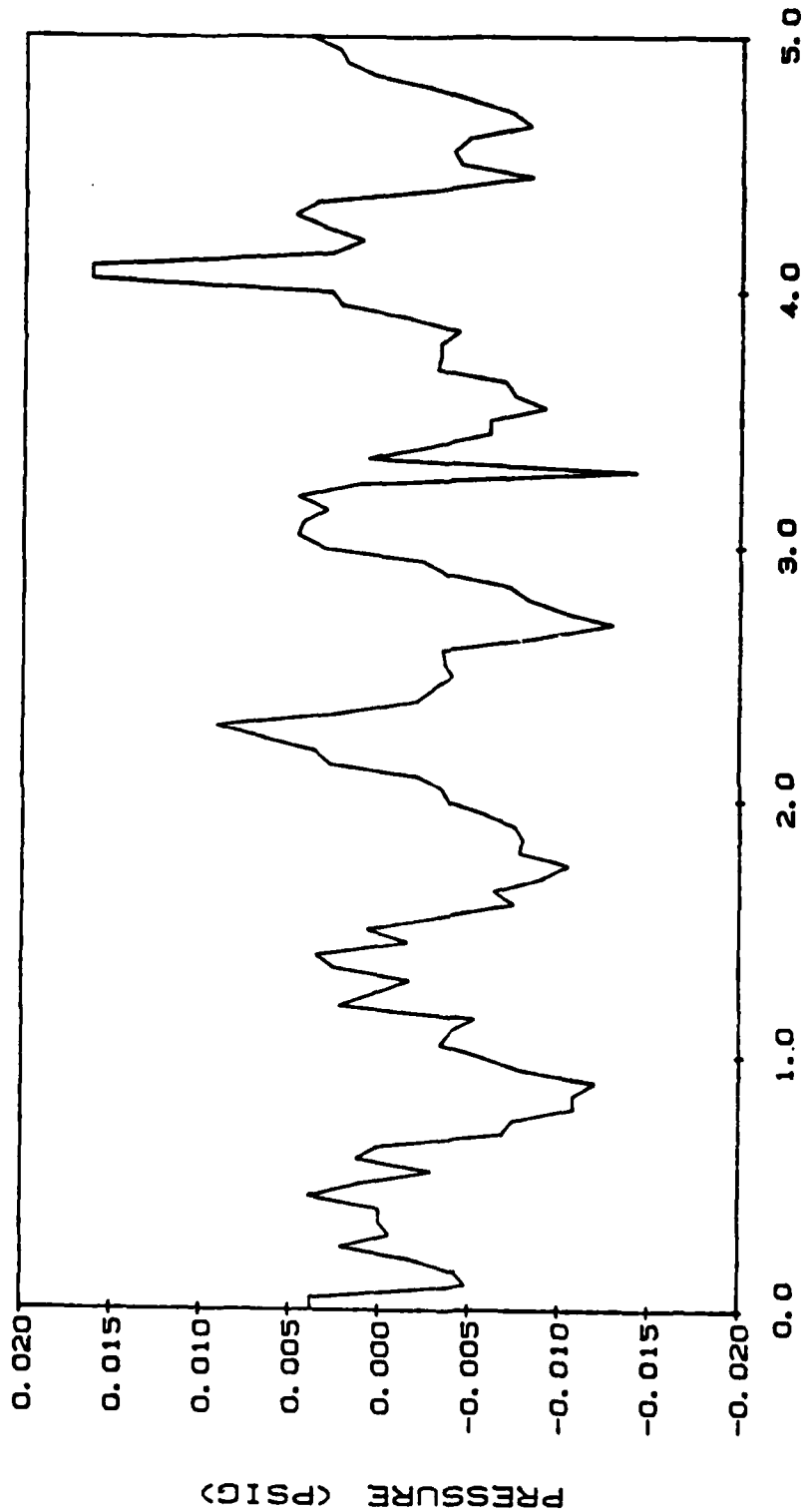

Figure 7. Digitized averaged pressure signal averaged over 1 rotor revolution

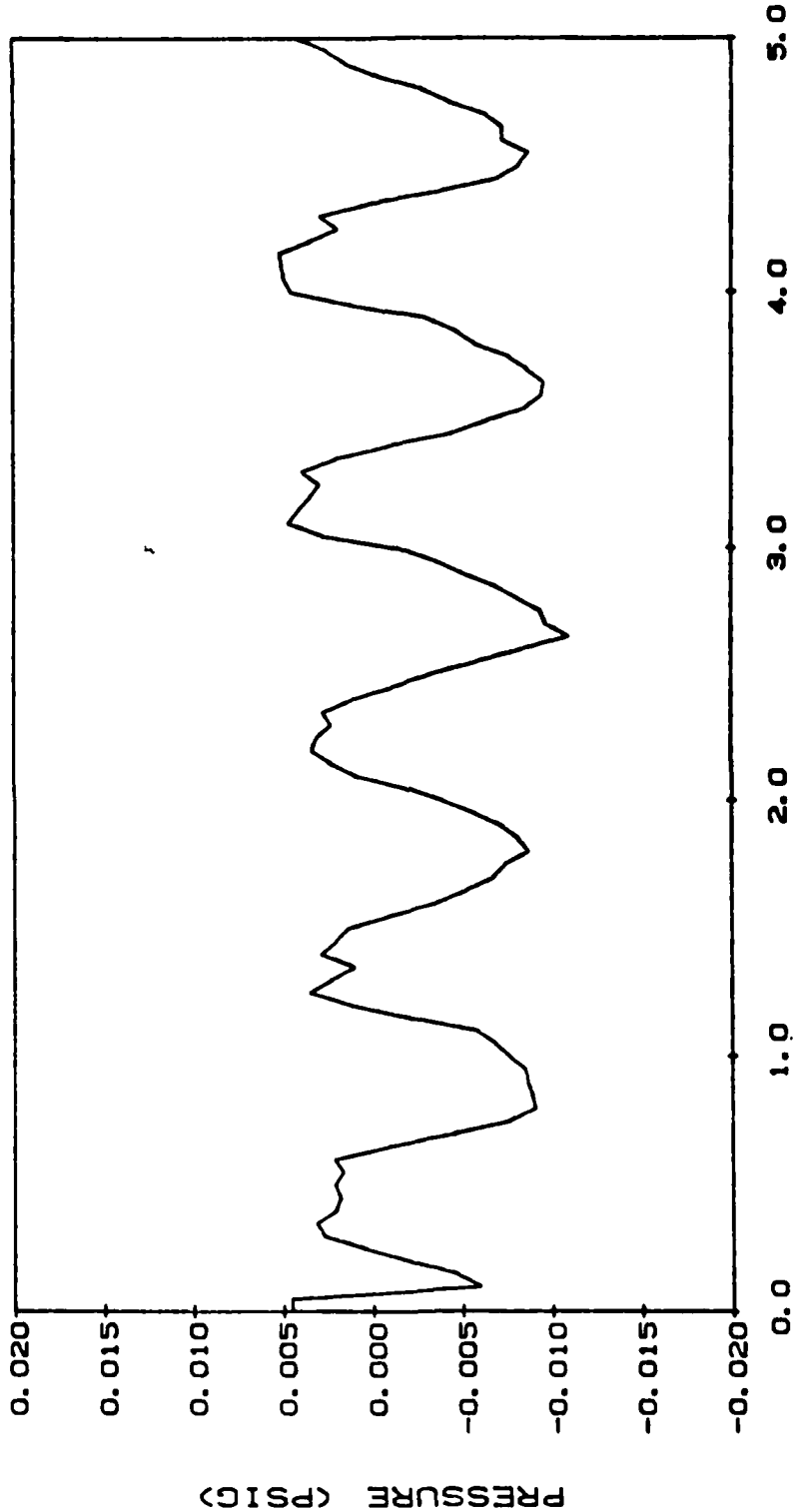

Figure 8. Digitized averaged pressure signal averaged over 25 rotor revolutions

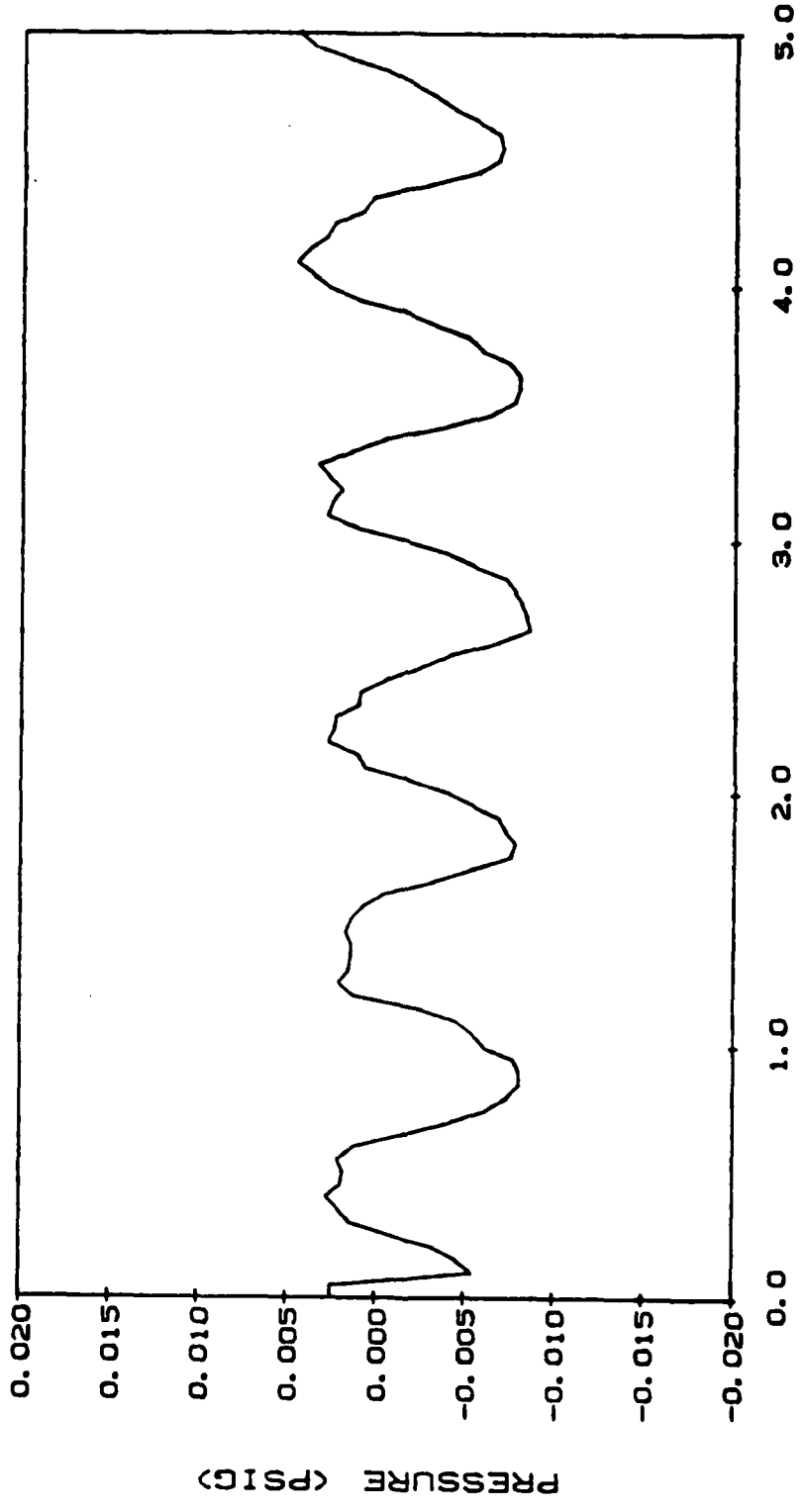

Figure 9. Digitized averaged pressure signal averaged over 50 rotor revolutions

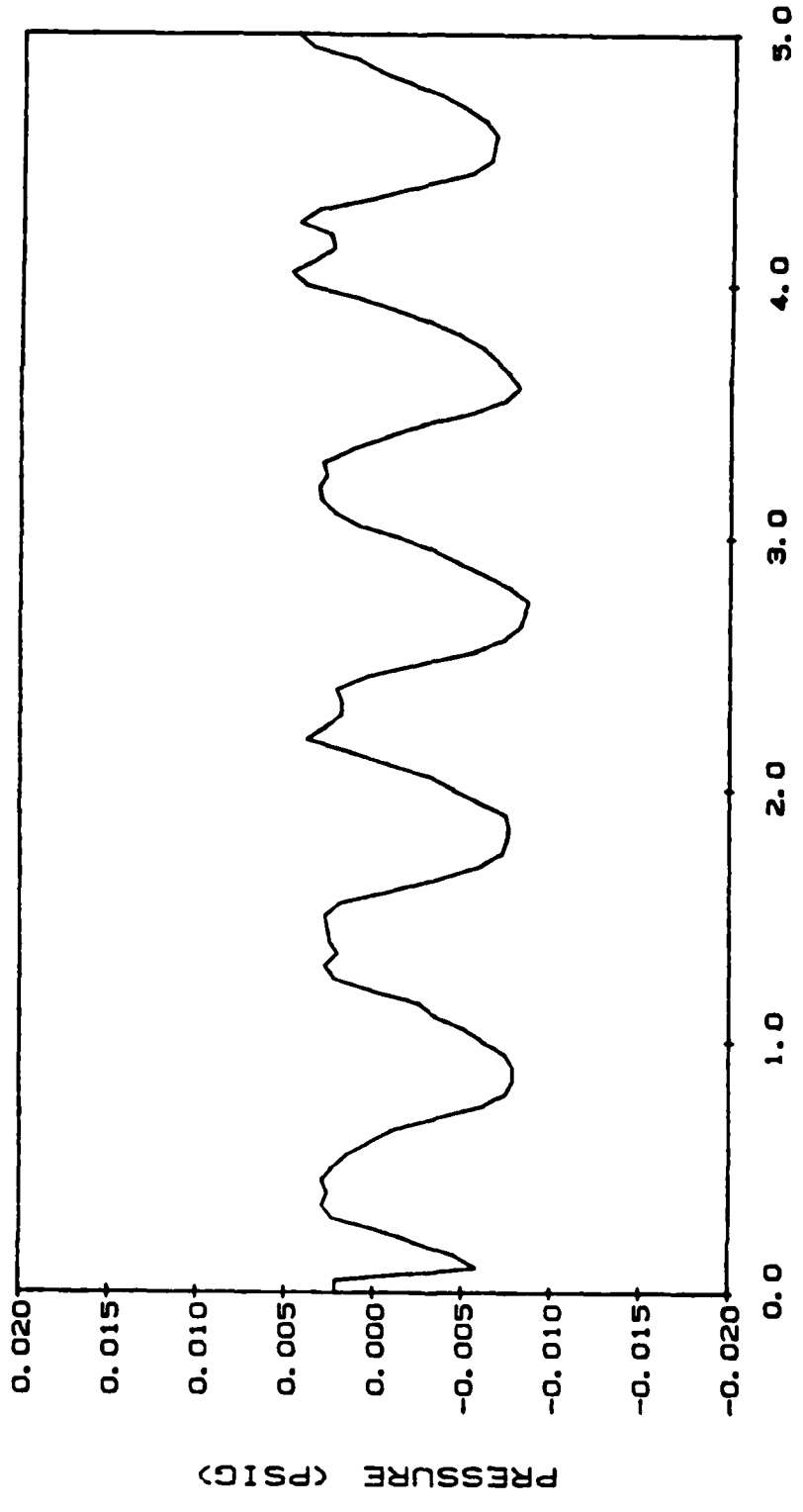

Figure 10. Digitized averaged pressure signal averaged over 75 rotor revolutions

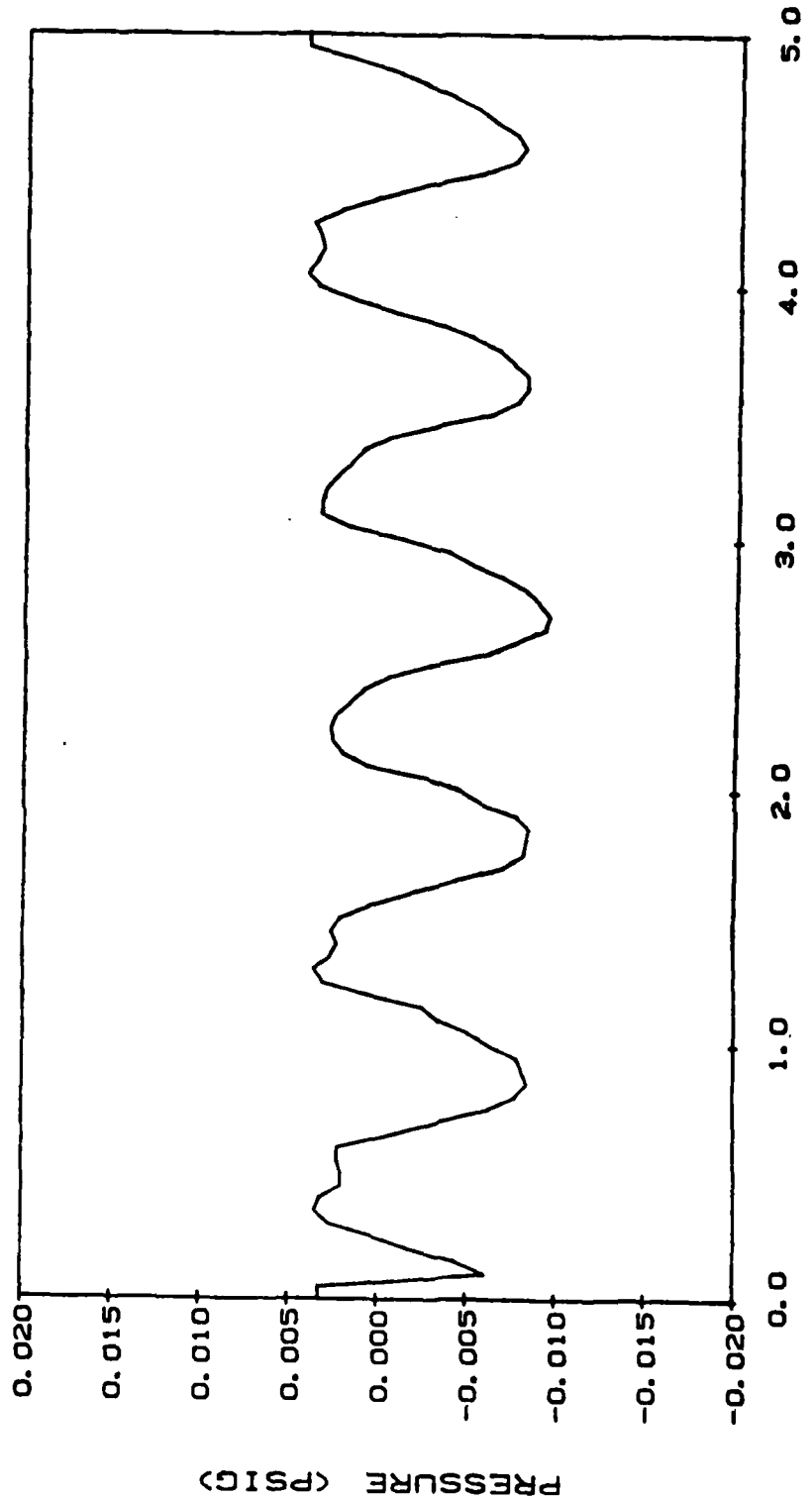

Figure 11. Digitized averaged pressure signal averaged over 100 rotor revolutions

pressure surface dynamic pressure transducer for 1 rotor revolution and averaged over 25, 50, 75, and 100 rotor revolutions, respectively. As seen, averaging greatly reduces the random fluctuations superimposed on the harmonic pressure signal of interest. Also, these time-variant pressure signals are essentially unchanged when averaged over 75 or more rotor revolutions, Figures 10 and 11. Thus, signal averaging for 100 rotor revolutions are used for the time-variant data acquisition of this initial check-out experiment.

At each steady-state operating point, an averaged time-variant data set, consisting of the Kulite dynamic pressure transducer signals digitized at a rate of 20 KHz and averaged over 100 rotor revolutions, was obtained. These rotor revolutions were not consecutive due to the finite time required for the A-D multiplexer system to sample the data and the computer to then read the digitized data. Figures 12 and 13 present typical examples of the digitized dynamic pressure signals at 14.1% chord on the vane pressure and suction surfaces, respectively.

Each of these digitized signals was Fourier decomposed into harmonics by means of an FFT algorithm. Figure 14 shows an example of this decomposition for the 14.1% chord pressure surface transducer signal at 73% span. As seen, the transducer signal contains a dominant fundamental frequency equal to the blade passing frequency and a smaller second harmonic component. In addition, the averaged signal exhibits minimal non-harmonic content. From this Fourier decomposition, both the magnitude of

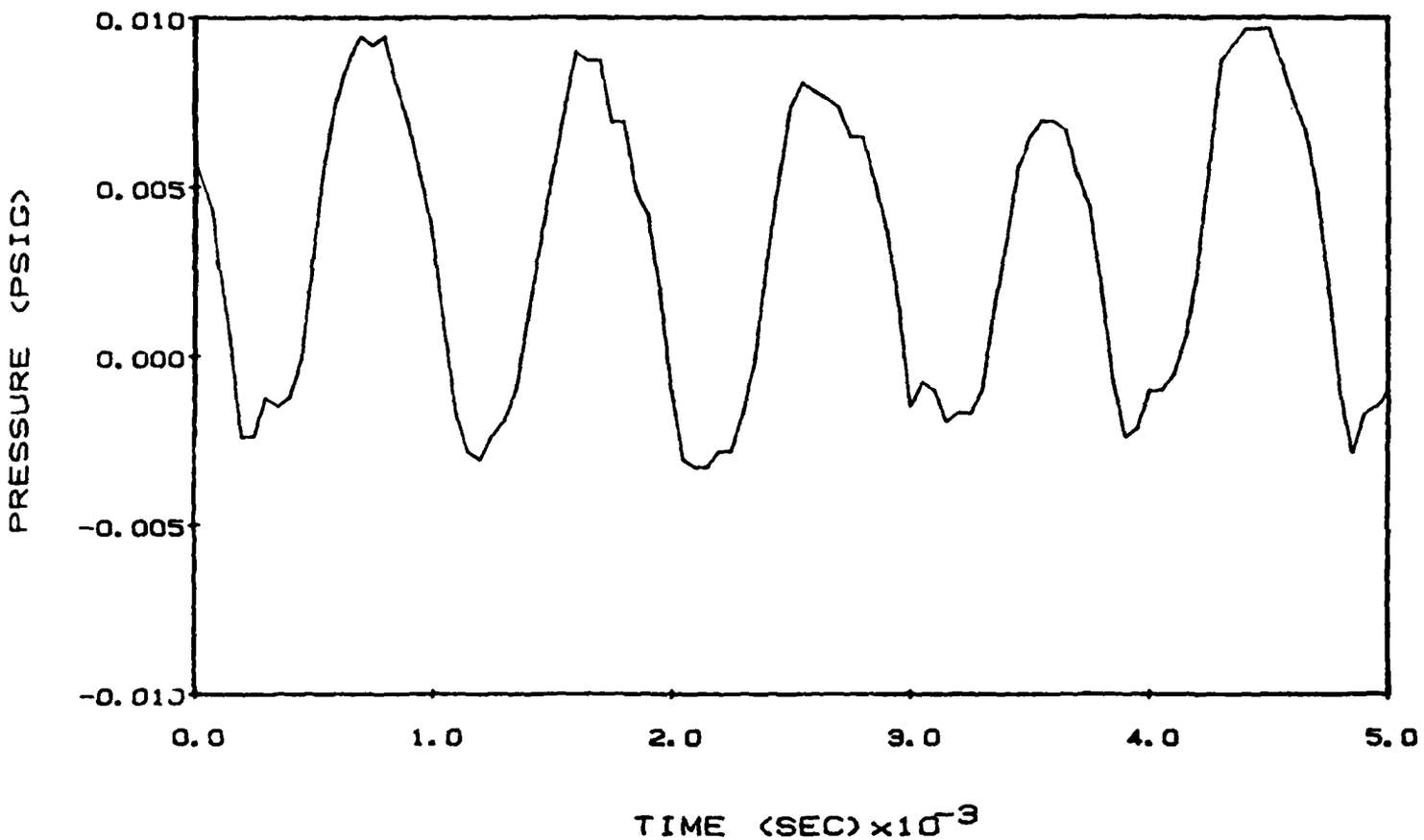

Figure 12. Digitized averaged pressure signal at 14.1% chord on the pressure surface

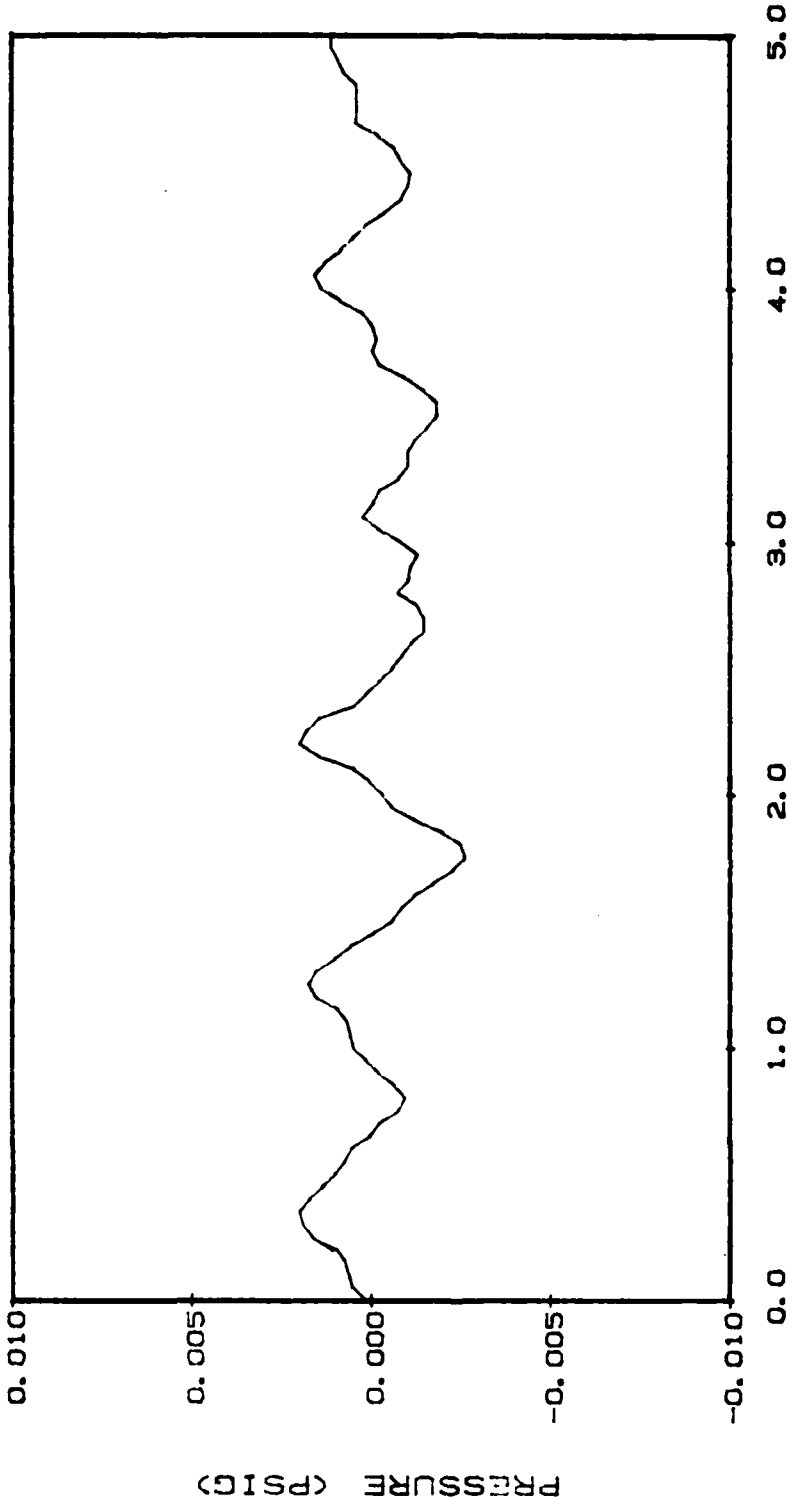

Figure 13. Digitized averaged pressure signal at 14.1% chord on the suction surface

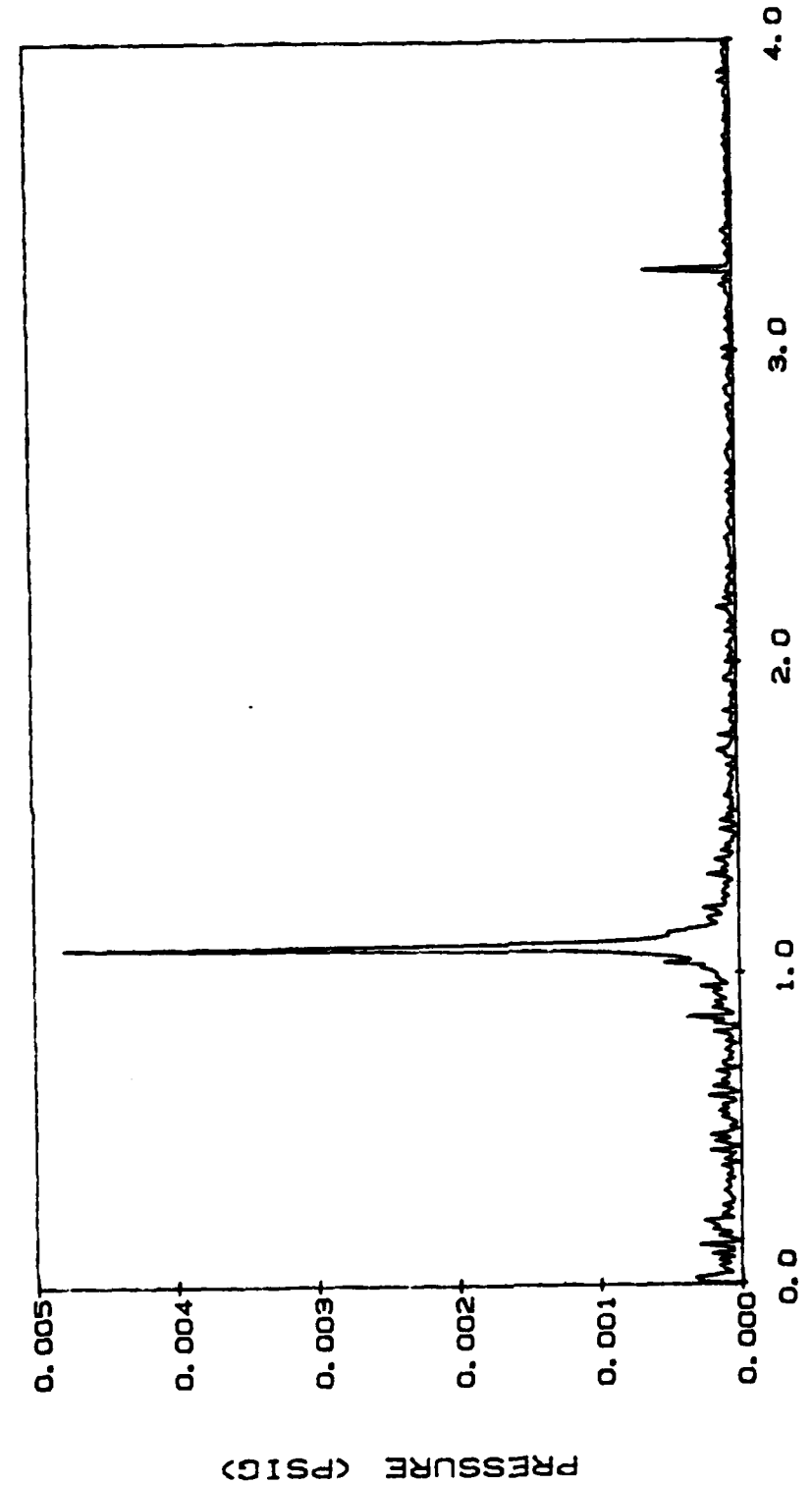

Figure 14. Fourier analysis of averaged pressure signal at 14.1% chord on the pressure surface

each component and its phase lag as referenced to the optical encoder pulse can be determined.

Cascade gust unsteady aerodynamic analyses predict the unsteady pressure difference across the vane as a function of airfoil chord in the form of a dynamic pressure difference coefficient and an aerodynamic phase lag. The dynamic pressure coefficient is normalized with respect to the steady-state properties of the flow and the magnitude of the transverse gust. The aerodynamic phase lag is referenced to a transverse gust at the leading edge of the reference airfoil. Hence, to enhance the experiment-theory correlation process, the data were adjusted in phase and magnitude to agree with the predictions at the leading edge transducer location. Thus, the final form of the dynamic data consists of a dynamic pressure coefficient and an aerodynamic phase lag. It should be noted that this adjustment in phase and magnitude will not be necessary in the ensuing experiments as a crossed hot-wire system will be used to quantify the forcing function.

Surface static pressure measurements on the 49.1% and the 73.0% span streamlines of the first stage stator vane quantify the steady-state aerodynamic chordwise loading distributions. Figure 15 presents these surface chordwise steady-state static pressure distributions.

As seen, at small negative incidence angle values, the aerodynamic loading distributions differ over the front portion of

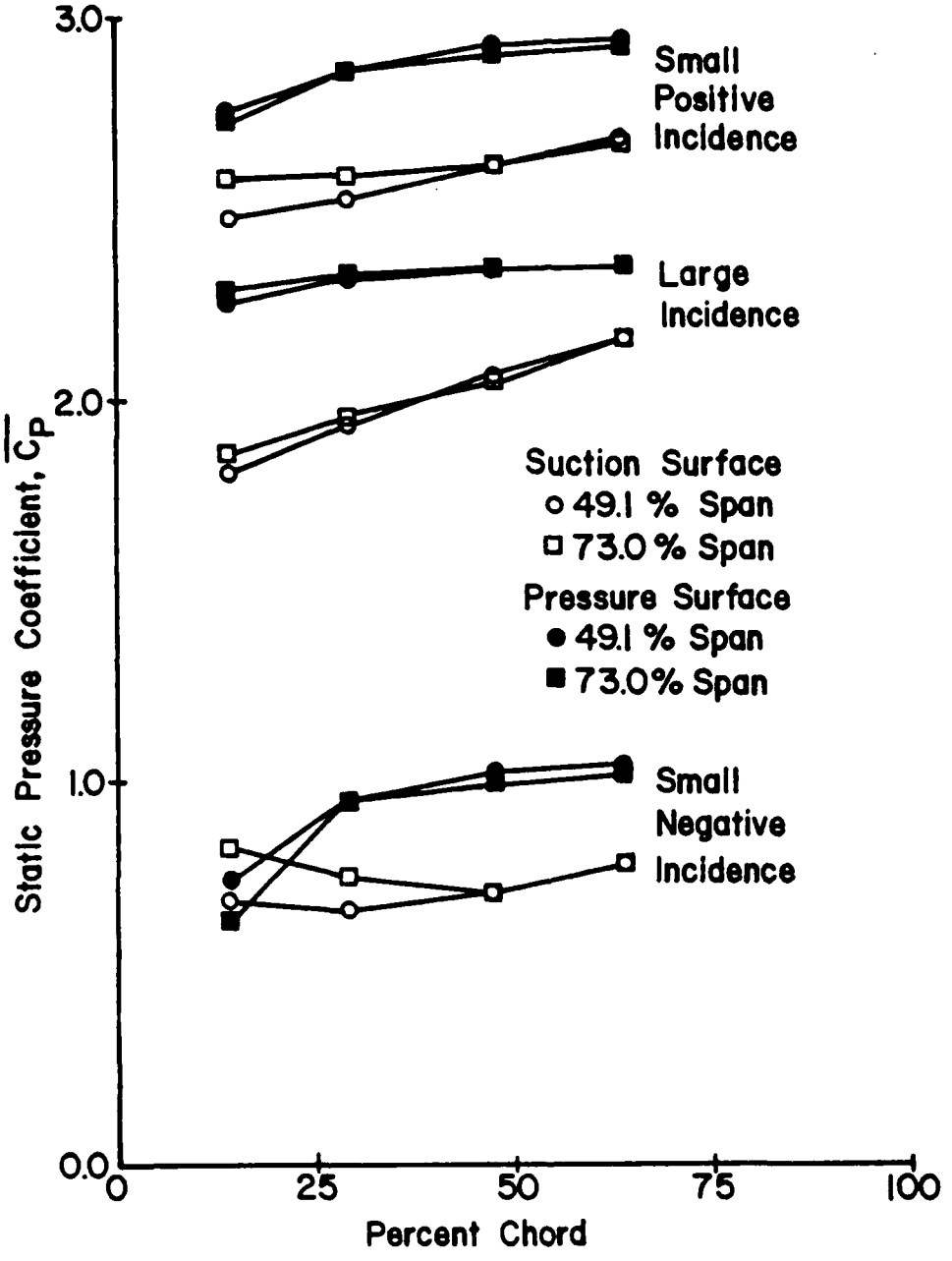

Figure 15. Airfoil static pressure coefficient as a function of airfoil chord

the chord, but coincide over the aft portion for these two spanwise streamlines. As the incidence angle is increased to small positive values, the pressure surface static pressure distributions coincide, but the suction surface distributions do not. At large positive incidence angle values, the two span streamline static pressure distributions are very nearly equal except for a slight deviation in the leading edge portion of the suction surface.

Figures 16 through 21 present the stator vane surface dynamic pressure coefficient and aerodynamic phase lag data for the first harmonic of the unsteady pressure difference across the vane as a function of percent airfoil chord. Also included in these figures are the predictions obtained from a compressible flow, small perturbation, flat plate airfoil cascade, transverse gust unsteady aerodynamic analysis. In this unique analysis, the effect of a specified steady-state separation on the airfoil suction surface is modeled by a thin slip region which extends from the specified separation point chordwise location to aft of the blade trailing edge.

Figures 16 and 17 present the small negative and positive incidence angle dynamic pressure data on the 73.0% span streamline. As seen, good correlation exists between the data and the unseparated predictions for the dynamic pressure coefficient. However, the aerodynamic phase lag data exhibit a somewhat different chordwise distribution than that of the prediction. In particular, the aerodynamic phase lag first increases and then

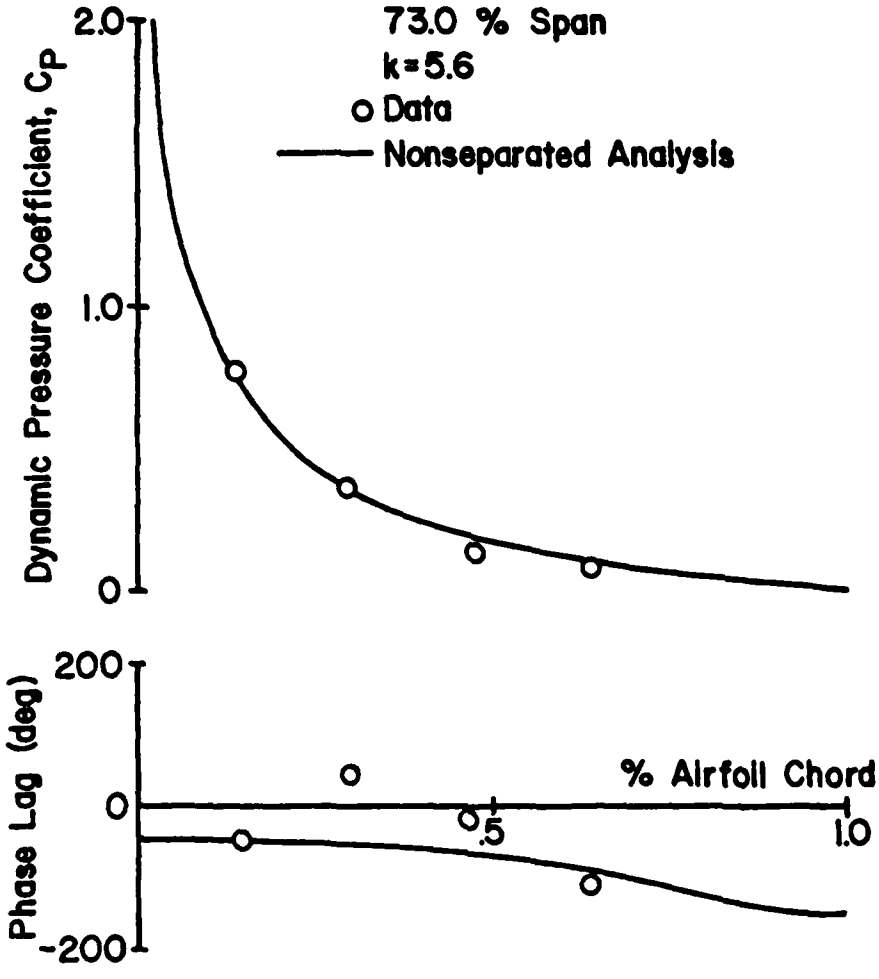

Figure 16. Chordwise variation of the dynamic pressure coefficient and aerodynamic phase lag at -1.9° of incidence

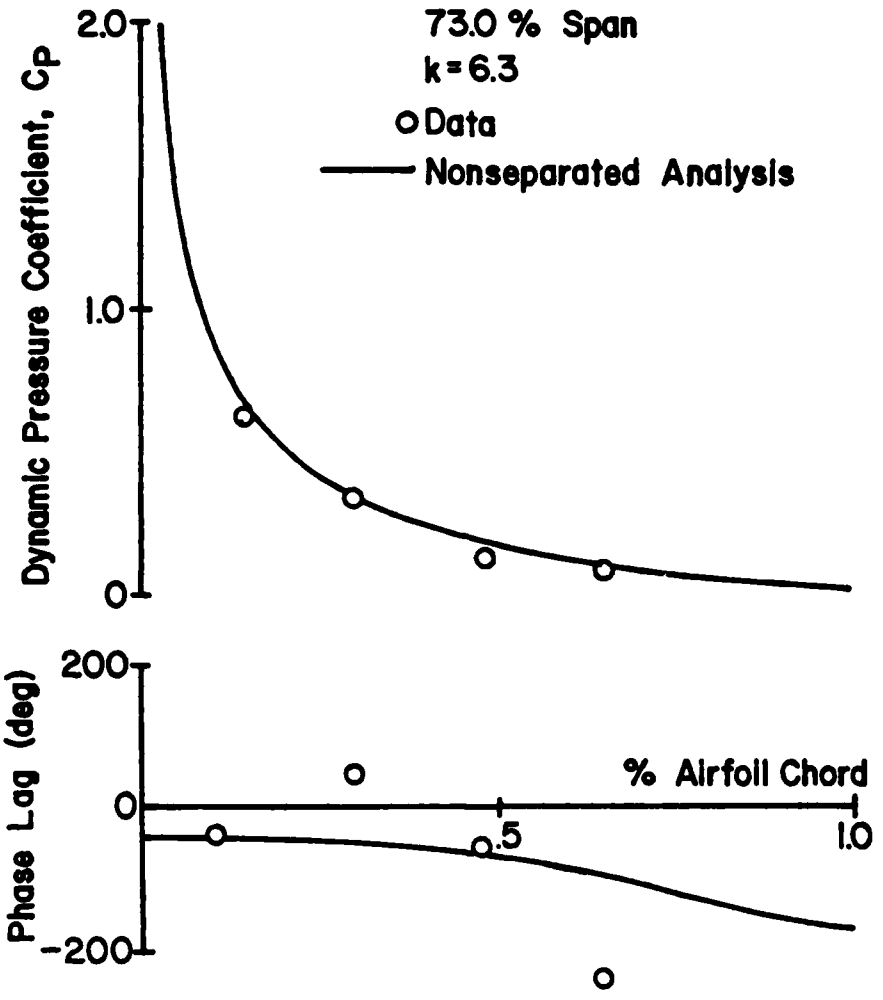

Figure 17. Chordwise variation of the dynamic pressure coefficient and aerodynamic phase lag at 3.6° of incidence

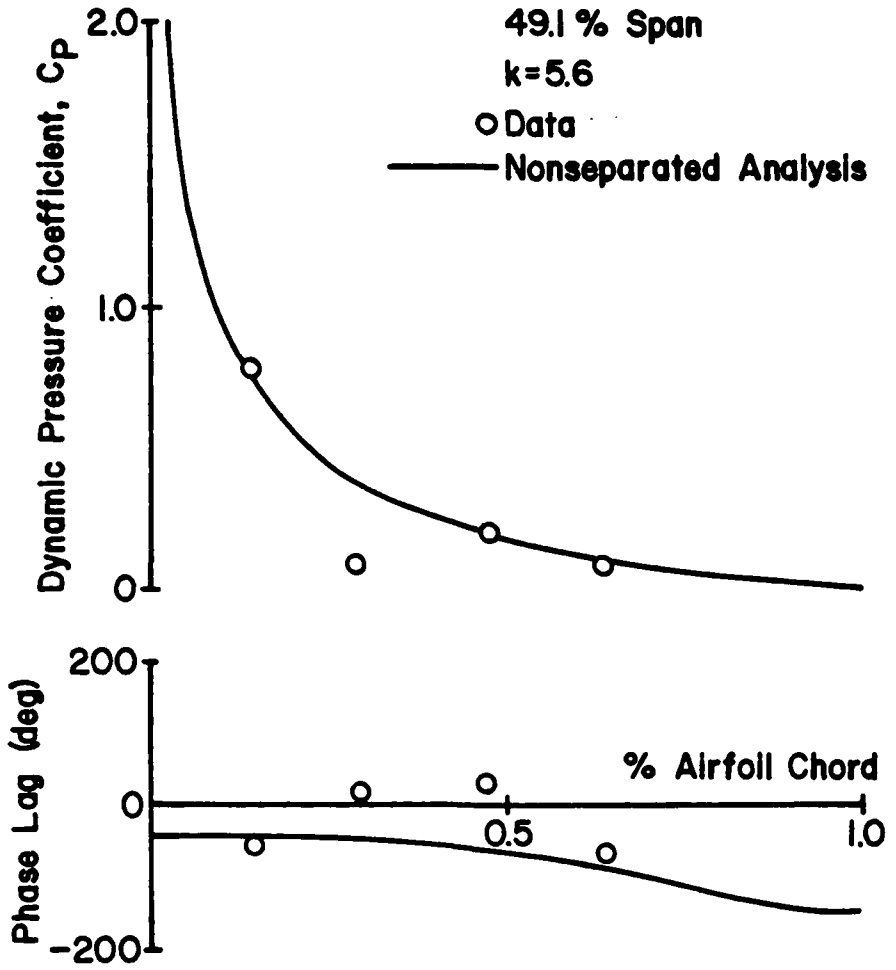

Figure 18. Chordwise variation of the dynamic pressure coefficient and aerodynamic phase lag at -1.0° of incidence

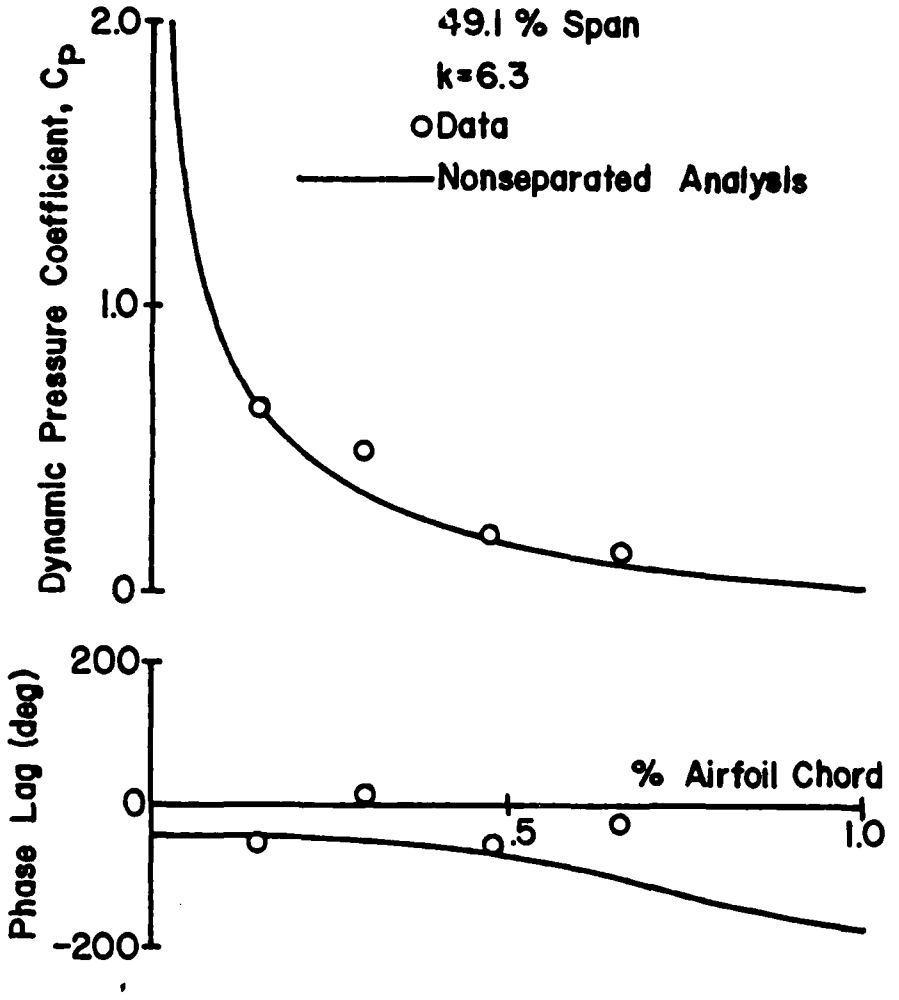

Figure 19. Chordwise variation of the dynamic pressure coefficient and aerodynamic phase lag at 3.5° of incidence

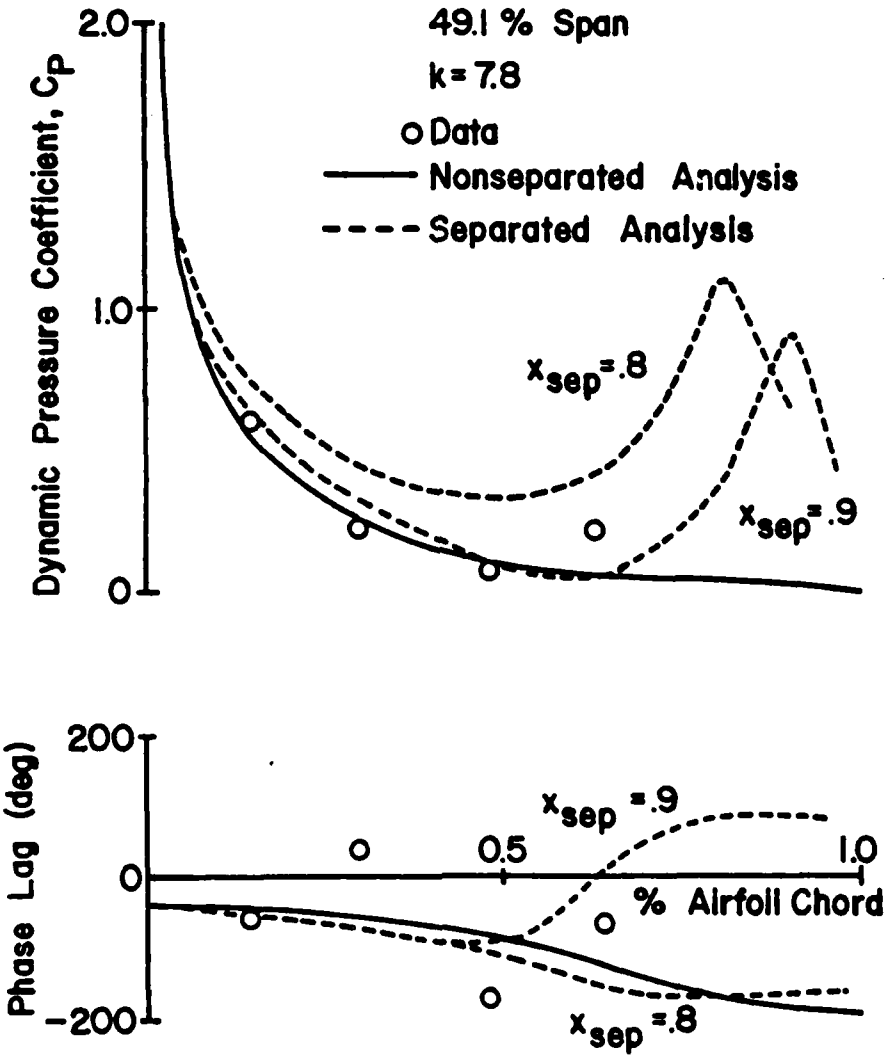

Figure 20. Chordwise variation of the dynamic pressure coefficient and aerodynamic phase lag at 10.5° of incidence

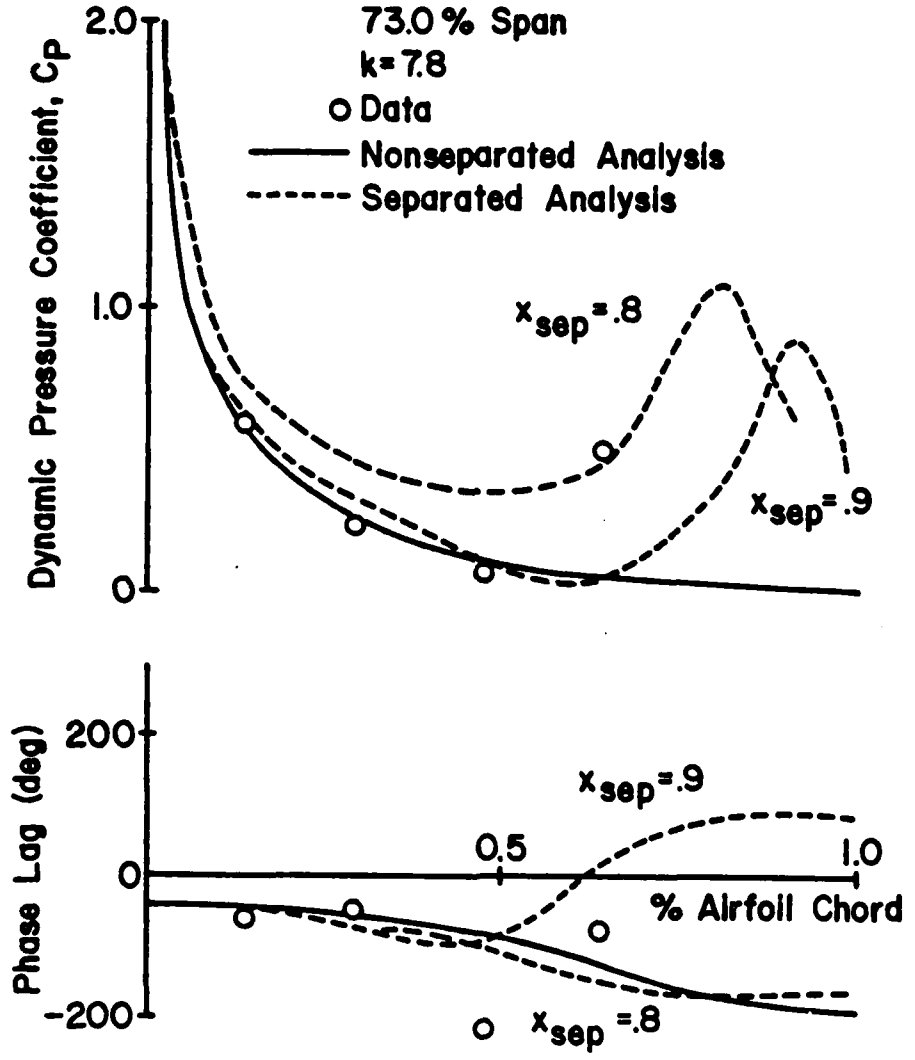

Figure 21. Chordwise variation of the dynamic pressure coefficient and aerodynamic phase lag at 11.7° of incidence

decreases as a function of chord, with the decrease being more pronounced as the incidence angle is increased. This chordwise variation in the aerodynamic phase lag data is attributed to the camber of the stator vane. The difference between the small negative and positive incidence angle phase lag distributions is due to the differences in the steady-state aerodynamic loading, as detailed in Figure 15.

The small negative and positive incidence angle results on the 49.1% span streamline are presented in Figures 18 and 19, respectively. As seen, at the small negative incidence angle, the aerodynamic phase lag data-theory correlation is very similar to the corresponding data on the 73.0% streamline. At the positive incidence angle, a larger decrease in the phase lag value at 63.7% chord is found. The dynamic pressure coefficient correlation at 49.1% span is generally good at both incidence angle values. However, the 29.1% chord data point is noticeably lower in value than the corresponding prediction at the negative incidence angle and increased in value over the prediction at the positive incidence angle value. These variations in the aerodynamic phase lag and the dynamic pressure coefficient data are due to the differences in the steady-state aerodynamic loading, as presented in Figure 15.

Figures 20 and 21 present the large positive incidence angle dynamic pressure data-theory correlation on the 49.1% and 73.0% span streamlines, respectively. Also included in these figures are the correponding unseparated and separated flow predictions.

Both sets of data exhibit analogous trends. As per the lower incidence angle results, the aerodynamic phase lag data first increase and then decrease relative to the predictions. Also, the aft region separated flow prediction indicates little effect on the predicted phase lag at this large reduced frequency value. The dynamic pressure coefficient chordwise data distribution exhibits the same trends as the separated flow predictions. In particular, the dynamic pressure coefficient data and predictions decrease as the chord position is increased over the front of the airfoil. However, while the nonseparated prediction continues to decrease over the aft part of the airfoil chord, the data and the separated flow predictions show increased values, with the higher incidence angle data exhibiting the largest increase, as seen in Figure 21.

Rotor Studies

The development of the dynamic instrumentation and calibration procedures for the first stage rotor blade studies has been initiated. Modifications to the rotor shaft to route lead wires to the slip ring assembly has been initiated. Also, a slip ring assembly has been selected and ordered. In addition, design has been initiated on the rotating signal conditioning system as well as the dynamic transducer installation on the rotor blades.

Analysis

the parametric study has been completed with the coupled mode blade vibration energy balance structural dynamics math model. These results are presented in the Appendix.

APPENDIX

THE COUPLED RESPONSE OF TURBOMACHINERY BLADING TO AERODYNAMIC EXCITATIONS

AIAA Journal of Aircraft

Volume 21, No. 4, April 1984

The Coupled Response of Turbomachinery Blading to Aerodynamic Excitations

Daniel Hoyniak* and Sanford Fleeter†
Purdue University, West Lafayette, Indiana

An energy balance technique is developed which predicts the coupled bending-torsion mode aerodynamic forced response of an airfoil. The effects of the various aerodynamic parameters are then considered utilizing a subsonic compressible flow/flat plate cascade gust analysis. The increased coupling between the torsion and translation modes as the natural frequencies approach one another is shown. It is also demonstrated that the coupled-response amplitudes increase with: 1) decreased structural damping, 2) increased solidity, stagger angle, and Mach numbers, 3) interblade phase angles corresponding to forward traveling waves, and 4) shifting of the elastic axis location aft.

Nomenclature

a = distance of elastic axis aft of mid-chord
A = unsteady lift influence coefficient
b = airfoil semichord (C/2)
B = unsteady moment influence coefficient
C = airfoil chord
C/S = cascade solidity (airfoil chord/airfoil spacing)
C_1 = $\mu x_\alpha + (A_\alpha)^R$
C_2 = $\mu x_\alpha + (B_h)^R$
C_3 = $[\mu - \mu(\omega_h/\bar{\omega})^2 + (A_h)^R]$
C_4 = $(A_h)^I - \mu(\omega_h/\bar{\omega})^2 g_h$
C_5 = $\mu r_\alpha^2[1 - (\omega_\alpha/\bar{\omega})^2] + (B_\alpha)^R$
C_6 = $(B_\alpha)^I - \mu r_\alpha^2(\omega_\alpha/\bar{\omega})^2 g_\alpha$
C_7 = $-(W_G/U)(A_G)^R$
C_8 = $-(W_G/U)(A_G)^I$
C_9 = $-(W_G/U)(B_G)^R$
C_{10} = $-(W_G/U)(A_G)^I$
D_I = $|(C_4C_5 + C_6C_3) - [C_3(A_\alpha)^I + C_1(A_h)^I]|$
D_R = $|(C_3C_5 - C_4C_6) - [C_3C_1 - (A_\alpha)^I(B_h)^I]|$
h = complex translational displacement
h_0 = amplitude of translational oscillation
i = $\sqrt{-1}$
I_α = mass moment of inertia per unit span about the elastic axis
k = reduced frequency ($k = \bar{\omega}b/U$)
L = unsteady lift
m = mass per unit span of the airfoil
M = unsteady moment
N_{hI} = $|(C_4C_5 + C_6C_7) - [C_9(A_\alpha)^I + C_1C_{10}]|$
N_{hR} = $|(C_7C_5 - C_8C_6) - [C_1C_9 - C_{10}(A_\alpha)^I]|$
$N_{\alpha I}$ = $|(C_{10}C_3 + C_8C_9) - [C_7(B_h)^I + C_2C_7]|$
$N_{\alpha R}$ = $|(C_3C_9 - C_8C_{10}) - [C_7C_2 - C_7(B_h)^I]|$
Re[ ] = real part of [ ]
r_α = radius of gyration about elastic axis
S_α = airfoil static moment per unit span about the elastic axis
U = freestream velocity
W = complex transverse gust function
W_G = amplitude of transverse gust
WORK = unsteady work per cycle of oscillation
x_α = location of center of gravity relative to elastic axis
α = complex torsional displacement
α_0 = amplitude of torsional motion
μ = mass parameter
ρ = fluid density
σ = interblade phase angle
ω = airfoil natural frequency
$\bar{\omega}$ = frequency of the transverse gust

Subscripts

G = gust
h = translation
SI = self-induced (aerodynamic damping)
α = torsion

Superscripts

I = imaginary part
R = real part
( ) = derivative with respect to time

Introduction

AERODYNAMICALLY-induced vibrations of rotor and stator airfoils are one of the more common sources of high-cycle fatigue failure in gas turbine engines. Destructive aerodynamic forced responses of fan, compressor, and turbine blading have been generated by a wide variety of sources including upstream blades and/or vanes, distortion, rotating stall, downstream blades and/or vanes, surge, bleeds, and random or otherwise unidentified sources.

Failure level vibratory responses occur when a periodic aerodynamic forcing function, with frequency equal to a natural blade resonant frequency, acts on a blade row. The rotor speeds at which these forced responses occur are predicted with Campell diagrams, which display the natural frequency of each blade mode vs rotor speed.[1] Whenever these curves cross, aerodynamically-induced forced responses are possible. However, at the present time no accurate prediction for the amplitude of the resulting stress can be made.

The prediction of the aerodynamic forced response vibratory behavior of a blade or vane row requires a definition of the unsteady forcing function in terms of its harmonics. The time-variant aerodynamic response of the

Presented as Paper 83-0844 at the AIAA/ASME/ASCE/AHS Structures, Structural Dynamics, and Materials Conference, Lake Tahoe, Nev., May 2-4, 1983; received May 13, 1983; revision received Oct. 3, 1983.

*Graduate Research Assistant; presently Aerospace Engineer, NASA Lewis Research Center, Cleveland, Ohio.

†Professor, School of Mechanical Engineering, and Director, Thermal Sciences and Propulsion Center. Member AIAA.

airfoil to each harmonic of this forcing function is then assumed to be comprised of two parts.[2] One part is due to the disturbance being swept past the non-responding fixed airfoils. The second arises when the airfoils respond to this disturbance. These effects are modeled by means of two distinct analyses. A linearized small-perturbation gust analysis is used to predict the time-variant aerodynamics of the fixed non-responding airfoil to each harmonic of the disturbance. A self-induced unsteady aerodynamic analysis, wherein the airfoils are assumed to be harmonically oscillating, is then used to predict the additional aerodynamic effect due to the airfoil response. These self-induced aerodynamic effects can be thought of as an aerodynamic damping which can be either positive or negative. Reviews of state-of-the-art unsteady aerodynamics as applied to turbomachines, including gust and self-induced unsteady aerodynamic analyses, are presented in Refs. 3 and 4.

The classical approach to the prediction of the aerodynamic forced response of an airfoil is based on Newton's second law. The gust and self-induced unsteady aerodynamic analyses are used to describe the harmonic forces and moments acting on the airfoil in conjunction with a lumped parameter description of the airfoil structural and inertial properties.[4]

An alternate approach based on an energy balance technique has been developed by Hoyniak and Fleeter[5] to predict the uncoupled single-degree-of-freedom forced response of an airfoil. In this approach, a balance is established between the energy of unsteady aerodynamic work and the energy dissipated by the airfoil.

The objective of this paper is to extend the energy balance technique to include the more interesting case of coupled bending-torsion mode forced response of an airfoil and, also, to demonstrate the effects of the various aerodynamic and structural parameters on this coupled response.

General Unsteady Aerodynamic Coefficients

Figure 1 presents a schematic representation of a two-dimensional airfoil section displaced in both torsion and translation in a uniform flow with a superimposed convected transverse sinusoidal gust. Equation (1) presents the complex, time-dependent unsteady lift and moment per unit span, written in influence coefficient form, for the gust response and the self-induced unsteady aerodynamic cases.

$$L_G = L_G^R + iL_G^I = \pi\rho b^2\bar{\omega}^2\left[A_G\left(\frac{W}{U}\right)\right]$$

$$M_G = M_G^R + iM_G^I = \pi\rho b^4\bar{\omega}^2\left[B_G\left(\frac{W}{U}\right)\right]$$

$$L_{SI} = L_{SI}^R + iL_{SI}^I = \pi\rho b^3\omega^2\left[A_h\frac{h}{b} + A_\alpha\alpha\right]$$

$$M_{SI} = M_{SI}^R + iM_{SI}^I = \pi\rho b^4\omega^2\left[B_h\frac{h}{b} + B_\alpha\alpha\right] \qquad (1)$$

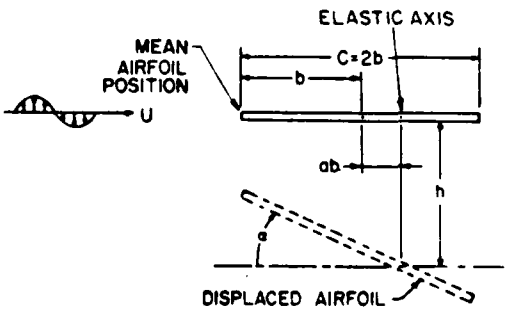

Fig. 1 Airfoil and displacement geometry and notation.

where $h = h_0 e^{i\bar{\omega}t}$; $\alpha = \alpha_0 e^{i\bar{\omega}t}$; $W = W_G e^{i\bar{\omega}t}$ describes the gust; (A_h, B_h), (A_α, B_α), (A_G, B_G) denote the generalized unsteady lift and moment coefficients due to airfoil translation, airfoil torsion, and the convected sinusoidal gust, respectively; ω is the airfoil natural frequency, and $\bar{\omega}$ is the gust forcing function frequency.

The total unsteady lift and moment on the airfoil are obtained by superimposing the gust response and the self-induced aerodynamic forces and moments.

$$L(t) = L_G(t) + L_{SI}(t)$$

$$= \pi\rho b^3\bar{\omega}^2\left[A_G\left(\frac{W_G}{U}\right) + A_h h_0 + A_\alpha\alpha_0\right]e^{i\bar{\omega}t}$$

$$M(t) = M_G(t) + M_{SI}(t)$$

$$= \pi\rho b^4\bar{\omega}^2\left[B_G\left(\frac{W_G}{U}\right) + B_h h_0 + B_\alpha\alpha_0\right]e^{i\bar{\omega}t} \qquad (2)$$

It should be noted that the airfoil response occurs at the frequency of the forcing function. Hence, in Eq. (2) the gust frequency $\bar{\omega}$ has been utilized in the specification of the unsteady aerodynamic forces and moments.

Energy Balance

The equations of motion describing the coupled translational and torsional displacement of the flat plate airfoil depicted in Fig. 1 are given in Eq. (3).

$$m\ddot{h} + S_\alpha\ddot{\alpha} + m\omega_h^2(1 + ig_h)h = L(t)$$

$$S_\alpha\ddot{h} + I_\alpha\ddot{\alpha} + I_\alpha\omega_\alpha^2(1 + ig_\alpha)\alpha = M(t) \qquad (3)$$

where m denotes the mass per unit span of the airfoil, S_α is the airfoil static moment per unit span about the elastic axis, ω_h and ω_α are the translational and torsional mode airfoil natural frequencies of the corresponding undamped single-degree-of-freedom system, respectively, and I_α is the mass moment of inertia per unit span about the elastic axis. As seen, the airfoil structural dynamic system described in Eq. (3) is strongly coupled and the coupling is associated with both the structural and the aerodynamic characteristics of the system. The structural coupling becomes significant whenever the aerodynamic center does not coincide with the elastic axis, in which case a non-zero value for the airfoil static moment results. The aerodynamic coupling arises because the self-induced aerodynamic forces acting on the airfoil are a function of the translational and torsional motions.

In this investigation, the coupled system response is determined utilizing an energy balance technique. The energy input to the system per cycle of airfoil oscillation is generated by the gust and, under certain conditions, the self-induced unsteady aerodynamic forces amd moments.[6] The energy dissipation of the system per cycle is associated with 1) system structural damping, 2) under certain conditions the self-induced aerodynamic forces and moments, and 3) the static moment term S_α. It should be noted that, for the uncoupled single-degree-of-freedom case, the dissipation term S_α was not considered.

The energy balance for the coupled translation-torsion airfoil motion can be expressed as follows.

$$(\text{WORK})_{SI}^h + (\text{WORK})_{g_h}^h + (\text{WORK})_G^h = (\text{WORK})_D^h$$

$$(\text{WORK})_{SI}^\alpha + (\text{WORK})_{g_\alpha}^\alpha + (\text{WORK})_G^\alpha = (\text{WORK})_D^\alpha \qquad (4)$$

where

$(WORK)^h_{SI}, (WORK)^\alpha_{SI}$ = work done by the self-induced aerodynamic forces and moments in translation and torsion, respectively.

$(WORK)^h_{g_h}, (WORK)^\alpha_{g_\alpha}$ = work done by the airfoil translation and torsion structural damping, respectively.

$(WORK)^h_{S_\alpha}, (WORK)^\alpha_{S_\alpha}$ = work associated with the static moment, S_α, in translation and torsion, respectively.

$(WORK)^h_G, (WORK)^\alpha_G$ = work done by the gust aerodynamic forces and moments in translation and torsion, respectively.

The work values associated with the self-induced unsteady aerodynamic forces and moments, $(WORK)^h_{SI}$ and $(WORK)^\alpha_{SI}$, have been written as dissipation terms. However, under certain conditions they may actually represent energy input terms. The sign differentiates between energy dissipation and input. Also, matrix techniques are utilized to solve Eq. (4) in order to determine the response of the airfoil system.

The unsteady work done by the self-induced aerodynamic terms, $(WORK)^h_{SI}$ and $(WORK)^\alpha_{SI}$, over one cycle of vibration can be calculated from Eq. (5).

$$(WORK)^h_{SI} = \oint \mathrm{Re}[L_{SI}(t)\,dh]$$

$$(WORK)^\alpha_{SI} = \oint \mathrm{Re}[M_{SI}(t)\,d\alpha] \qquad (5)$$

where $L_{SI}(t)$ and $M_{SI}(t)$ denote the unsteady lift and moment associated with the self-induced harmonic motion of the airfoil [See Eq. (1)].

Carrying out the integrations specified by Eqs. 1 and 5 results in the following expressions for the unsteady work done by the self-induced aerodynamic forces and moments.

$$(WORK)^h_{SI} = \pi^2 \rho b^3 \bar{\omega}^2 [-(A_h)^I h_0^2/b + (A_\alpha)^R h_0\alpha_0 \times \sin(\lambda_h - \lambda_\alpha) - (A_\alpha)^I h_0\alpha_0 \cos(\lambda_h - \lambda_\alpha)]$$

$$(WORK)^\alpha_{SI} = \pi^2 \rho b^4 \bar{\omega}^2 \left[(B_h)^R \left(\frac{h_0\alpha_0}{b}\right)\sin(\lambda_h - \lambda_\alpha) - (B_h)^I \left(\frac{h_0\alpha_0}{b}\right)\cos(\lambda_h - \lambda_\alpha) - (B_\alpha)^I \alpha_0^2\right] \qquad (6)$$

The angle λ_h denotes the phase angle between the incoming gust and the resulting translational motion of the airfoil. Similarly, the angle λ_α is the phase angle between the incoming gust and the airfoil torsional motion.

The energy input to the airfoil is determined by calculating the work per cycle of oscillation of the unsteady lift and moment associated with the incoming gust.

$$(WORK)^h_G = -\oint \mathrm{Re}[L_G(t)\,dh] = -\pi\rho b^3 \bar{\omega}^2 h_0 [(A_G)^I \cos(\lambda_h) - (A_G)^R \sin(\lambda_h)]$$

$$(WORK)^\alpha_G = \oint \mathrm{Re}[M_G(t)\,d\alpha] = \pi\rho b^4 \bar{\omega}^2 \alpha_0 [(B_G)^I \cos(\lambda_\alpha) - (B_G)^R \sin(\lambda_\alpha)] \qquad (7)$$

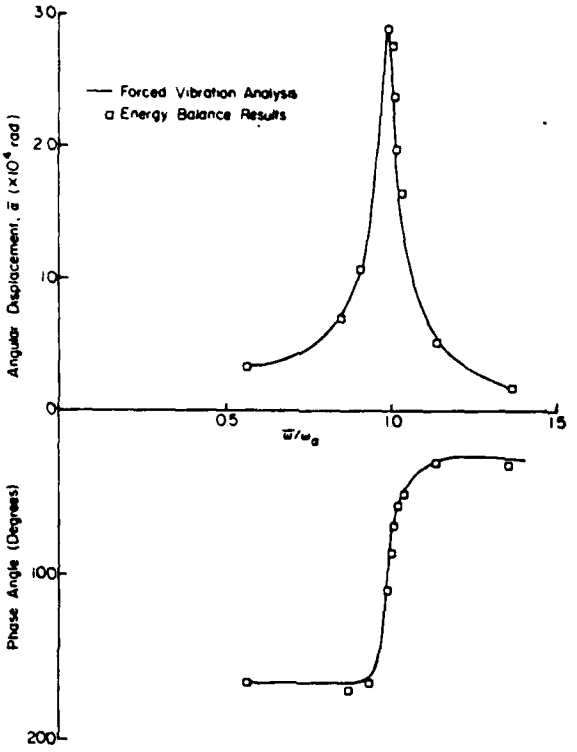

Fig. 2 Comparison of classical and energy balance forced response calculations.

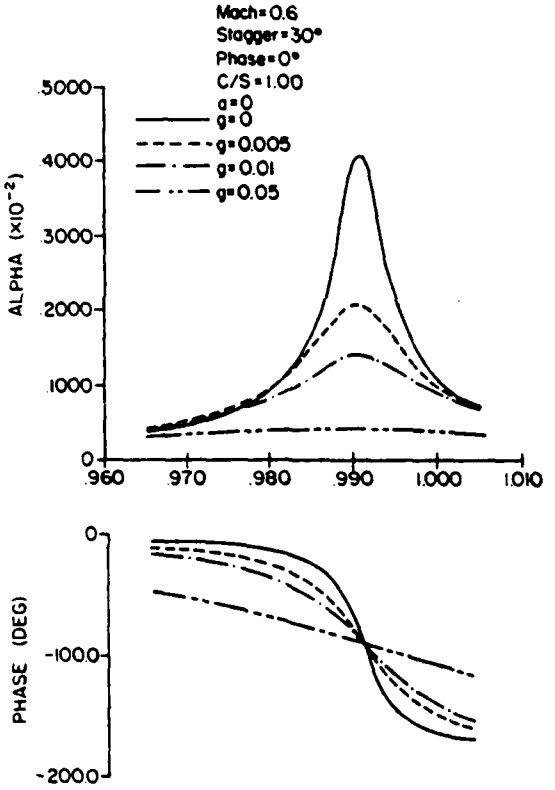

Fig. 3 Structural damping effect on the coupled torsional response amplitude for $(\bar{\omega}/\omega_\alpha)$ near ω_α.

The energy dissipated by the structural damping over one cycle of oscillation can be calculated as follows.

$$(\text{WORK})^{h}_{g_h} = \oint \text{Re}[ig_h m\omega_h^2 h\,dh] = \pi g_h m\omega_h^2 h_0^2$$

$$(\text{WORK})^{\alpha}_{g_\alpha} = \oint \text{Re}[ig_\alpha I_\alpha \omega_\alpha^2 \alpha\,d\alpha] = \pi g_\alpha I_\alpha \omega_\alpha^2 \omega_0^2 \qquad (8)$$

The unsteady work associated with the static moment S_α merits some additional comment. This is the term which couples the system equations of motion when the elastic axis and the aerodynamic center do not coincide. Physically, the S_α term can be considered as either a torsional force applied to the airfoil as the result of a unit translation airfoil displacement, or as a translational force resulting from the application of a unit torsional displacement. Thus, for an airfoil undergoing a translation mode oscillation, there is an apparent torsional load that can either do work on or extract work from the airfoil system. The phase relationship between the translational and torsional displacement determines whether this apparent torsional load adds or dissipates energy in the airfoil system.

The unsteady work per cycle of oscillation associated with the static moment can be determined by Eq. (9).

$$(\text{WORK})^{h}_{S_\alpha} = \oint \text{Re}[S_\alpha \ddot{\alpha}\,dh] = S_\alpha \bar{\omega}^2 \alpha_0 h_0 \pi \sin(\lambda_h - \lambda_\alpha)$$

$$(\text{WORK})^{\alpha}_{S_\alpha} = \oint \text{Re}[S_\alpha \ddot{h}\,d_\alpha] = S_\alpha \bar{\omega}^2 \alpha_0 h_0 \sin(\lambda_\alpha - \lambda_h) \qquad (9)$$

The substitution of the various work expressions into the energy balance [see Eq. (4)] yields the following matrix expression for the coupled translational and torsional airfoil displacements.

$$\begin{bmatrix} A_{11} & A_{12} \\ A_{21} & A_{22} \end{bmatrix} \begin{bmatrix} \left(\frac{h_0}{b}\right) \\ (\alpha_0) \end{bmatrix} = \begin{bmatrix} B_{11} \\ B_{21} \end{bmatrix} \qquad (10)$$

where

$$A_{11} = [\pi g_h m\omega_h^2 b] + [(A_h)^I \pi^2 \rho b^3 \bar{\omega}^2]$$

$$A_{12} = [S_\alpha \bar{\omega}^2 \pi - (A_\alpha)^R \pi^2 \rho b^3 \bar{\omega}^2] \sin(\lambda_h - \lambda_\alpha) + [(A_\alpha)^I \pi^2 \rho b^3 \bar{\omega}^2 \cos(\lambda_h - \lambda_\alpha)]$$

$$A_{21} = [S_\alpha \bar{\omega}^2 \pi - (B_h)^R \pi^2 \rho b^4 \bar{\omega}^2] \sin(\lambda_\alpha - \lambda_h) + [(B_h)^I \pi^2 \rho b^4 \bar{\omega}^4 \cos(\lambda_h - \lambda_\alpha)]$$

$$A_{22} = \pi g_\alpha I_\alpha \omega_\alpha^2 + (B_\alpha)^I \pi \rho b^4 \bar{\omega}^2$$

$$B_{11} = -\pi \rho b^3 \bar{\omega}^2 \left(\frac{W_G}{U}\right)[(A_G)^I \cos(\lambda_h) - (A_G)^R \sin(\lambda_h)]$$

$$B_{21} = \pi^2 \rho b^4 \bar{\omega}^2 \left(\frac{W_G}{U}\right)[(B_G)^I \cos(\lambda_\alpha) - (B_G)^R \sin(\lambda_\alpha)]$$

The phase angles between the translational and torsional displacements, λ_h and λ_α respectively, can be determined in various ways. For example, they can be determined directly from the classical solution of the coupled system equations of motion, Eq. (3) (see Ref. 5). For convenience and brevity, these phase angle relationships are presented in Eq. (11).

$$\lambda_h = \tan^{-1}\left[\frac{N_{hI} D_R - N_{hR} D_I}{N_{hR} D_R + N_{hI} D_I}\right]$$

$$\lambda_\alpha = \tan^{-1}\left[\frac{N_{\alpha I} D_R - N_{\alpha R} D_I}{N_{\alpha R} D_R + N_{\alpha I} D_I}\right] \qquad (11)$$

where N_{hI}, $N_{\alpha I}$, N_{hR}, $N_{\alpha R}$, D_R and D_I are defined in terms of the airfoil structural properties and the unsteady aerodynamic forces and moments in the Nomenclature.

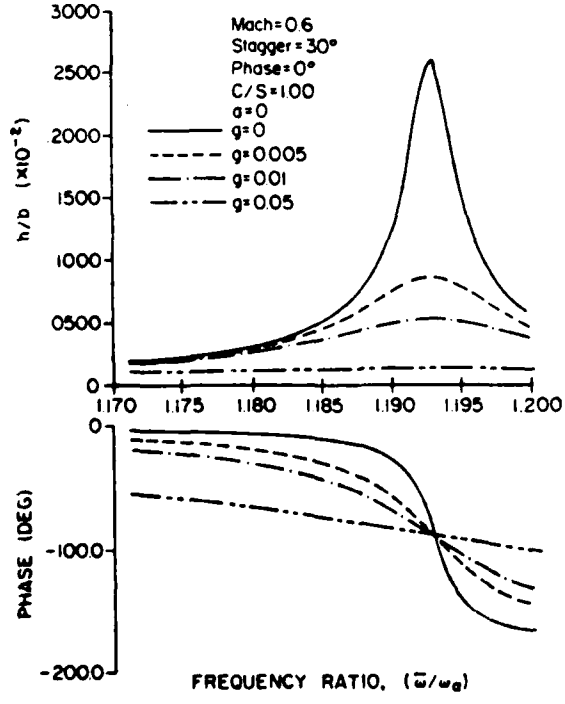

Fig. 4 Structural damping effect on the coupled torsional response for $(\bar{\omega}/\omega_\alpha)$ near ω_h.

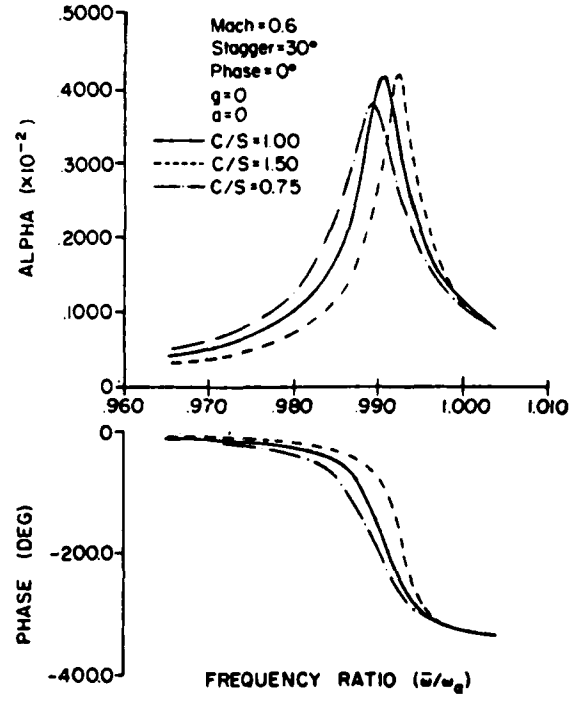

Fig. 5 Cascade solidity effect on the coupled torsional response.

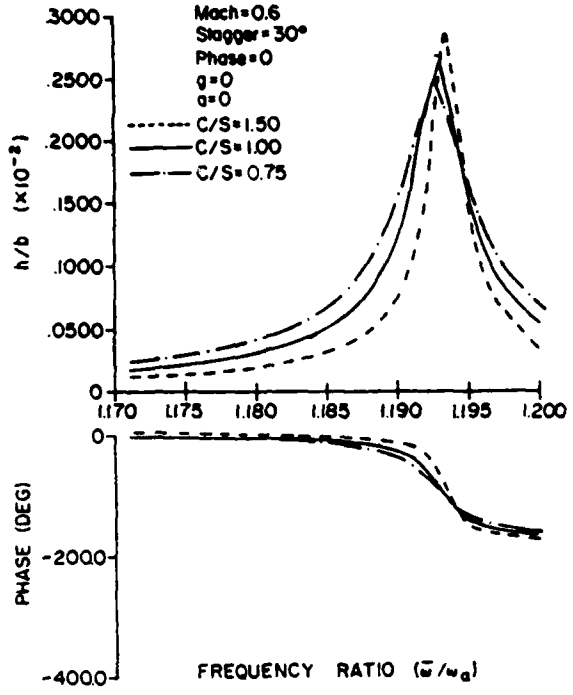

Fig. 6 Cascade solidity effect on the coupled translational response.

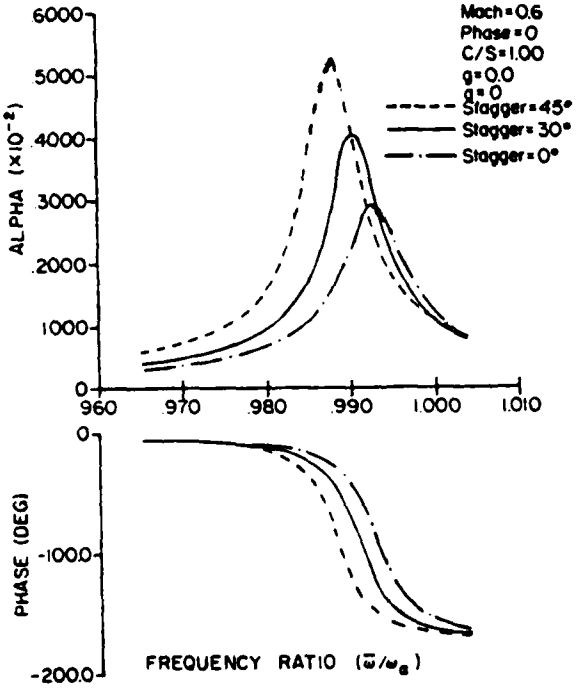

Fig. 7 Effect of stagger angle on the coupled torsional response.

Unsteady Aerodynamic Forces and Moments

L_h, M_h, L_α and M_α denote the standard form for the unsteady aerodynamic forces and moments and represent the unsteady lift and moment in translation and torsion, respectively, calculated about the airfoil ¼ chord. These standard form ¼ chord coefficients are related to the general unsteady aerodynamic influence coefficients through the following relationships.

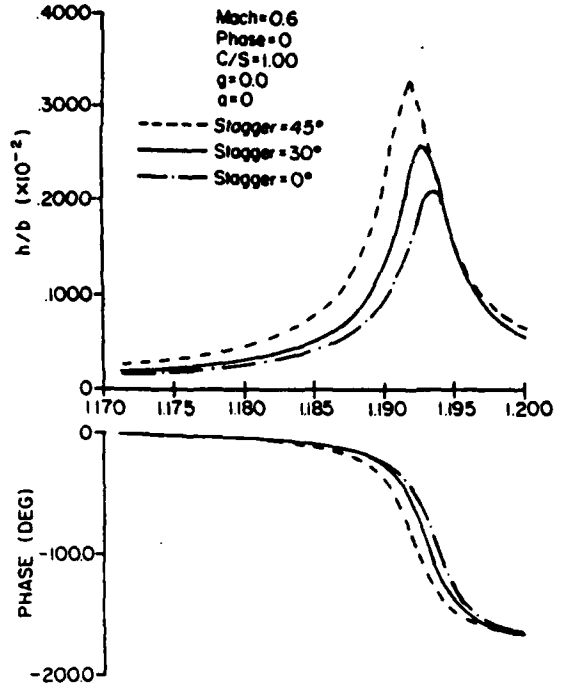

Fig. 8 Effect of stagger angle on the coupled translational response.

$$A_h = L_h$$

$$A_\alpha = L_\alpha - (\tfrac{1}{2}+a)L_h$$

$$A_G = L_H$$

$$B_h = M_h - (\tfrac{1}{2}+a)L_h$$

$$B_\alpha = M_\alpha - (\tfrac{1}{2}+a)(L_\alpha + M_h) + (\tfrac{1}{2}+a)^2 L_h$$

$$B_G = M_H \qquad (12)$$

where a is the dimensionless distance of the elastic axis measured from the airfoil mid-chord (see Fig. 1).

Results

To demonstrate the effects of the various parameters on the coupled forced response of turbomachinery blading, the unsteady aerodynamic analysis of Ref. 7 will be utilized. This analysis predicts the gust and self-induced unsteady aerodynamic forces and moments in a compressible flow field. The structural properties for this parametric study are based on an airfoil with a 5.08-cm chord, a 4% thickness-to-chord ratio, and an aspect ratio of 3. This representative airfoil has a natural translation mode frequency, ω_h, 12% larger than the natural torsion mode frequency, ω_α. Hence, $\omega_h/\omega_\alpha = 1.12$. Specific parameters to be varied include the structural damping value, the cascade solidity, the interblade phase angle, the inlet Mach number, and the elastic axis location. In addition, to clearly demonstrate the coupling effects, the airfoil stiffness is varied so as to make the torsional and translation mode natural frequencies nearly equal in value.

To verify the energy-balance approach for the prediction of aerodynamically-induced vibrations, the uncoupled torsion mode response of the representative airfoil was calculated by means of both the energy balance technique and a classical Newton's second law approach.[5] Figure 2 presents the comparison of these calculation techniques. As shown, the two methods yield identical results, both in terms of the amplitude and the phase of the response.

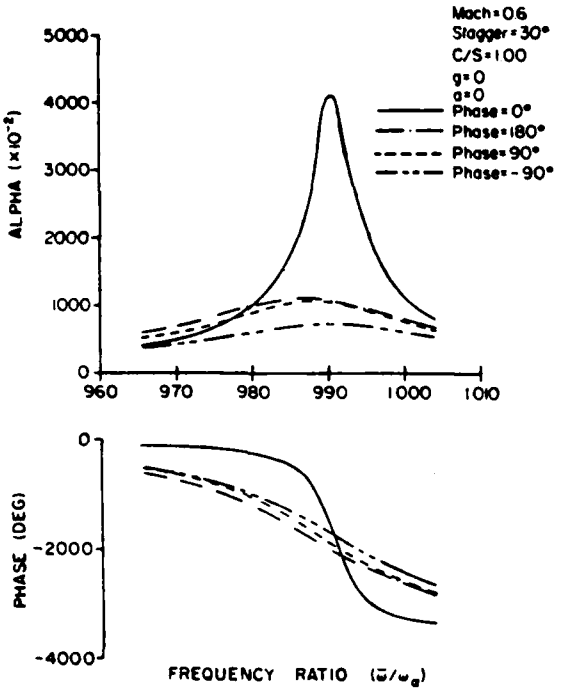

Fig. 9 Effect of interblade phase angle on the coupled torsion mode response.

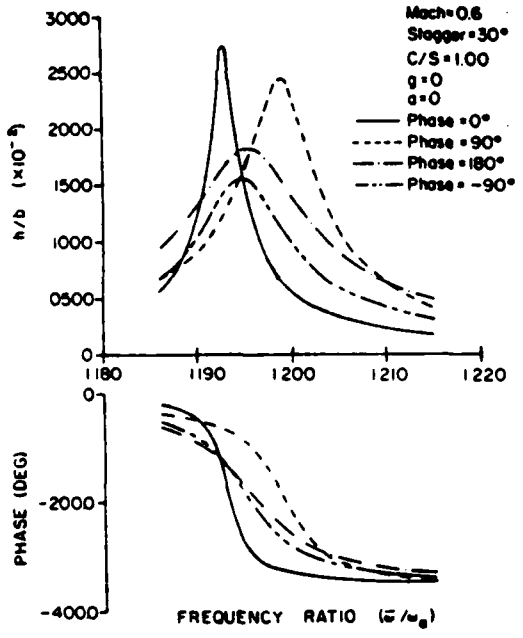

Fig. 10 Effect of interblade phase angle on the coupled translation mode response.

The coupled forced response characteristics of the representative airfoil are determined utilizing this energy balance technique. Results are presented as a function of the nondimensional ratio of the gust forcing frequency to the airfoil natural torsion mode frequency, $\bar{\omega}/\omega_\alpha$. Hence, values of 1.00 and 1.12 for this nondimensional frequency ratio correspond to the situations where the forcing function frequency is equal to the natural torsion and translation mode

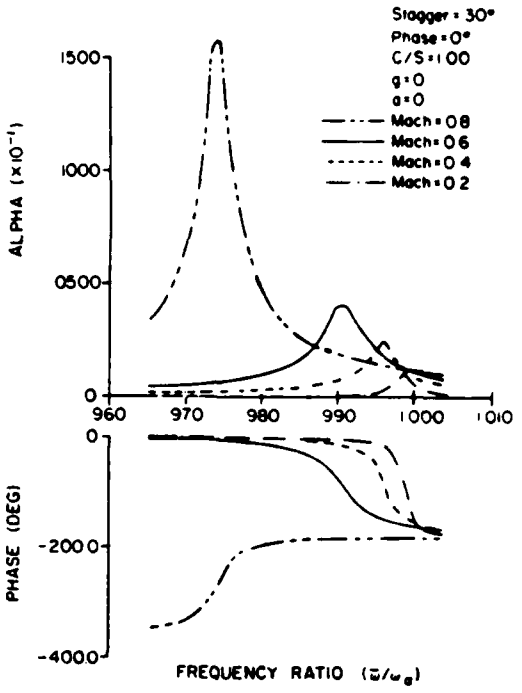

Fig. 11 Inlet Mach number effect on the coupled torsional response.

frequencies, respectively, of the representative airfoil. Results presented include the translational amplitude, the torsion mode amplitude, and the phase angles between the aerodynamic forcing function and the resulting airfoil response as a function of the nondimensional frequency ratio.

As anticipated, when the gust forcing function frequency is close to the natural torsion mode frequency, the torsional response is an order of magnitude greater than the corresponding coupled translation mode response. Thus, only the coupled forced torsional response will be presented for the forcing function close to the airfoil natural torsional frequency ($\bar{\omega}/\omega_\alpha \approx 1.00$), and only the coupled forced translational response for forcing function frequencies near the natural translational frequency ($\bar{\omega}/\omega_\alpha \approx 1.12$) will be presented.

Figures 3 and 4 represent the torsional and translational airfoil responses, respectively, with structural damping as the parameter when the forcing frequency is close to ω_α and ω_h, respectively. As seen, increased structural damping resulting results in decreased amplitude of response. It should be noted that the maximum response amplitudes do not occur at frequency ratio values of 1.00 and 1.12, even for the special case of zero structural damping. This is a result of the self-induced unsteady aerodynamic forces which correspond in this case to aerodynamic damping. Thus, even when there is no structural damping in the airfoil system, the self-induced aerodynamics generate aerodynamic damping.

The effects of cascade solidity (C/S) and stagger angle on the coupled forced response amplitudes are demonstrated in Fig. 5 and 6 and Figs. 7 and 8, respectively. Both the coupled torsional and translational forced response amplitudes increase with increasing values for solidity and stagger angle. Variations in solidity result in a somewhat more pronounced effect on the translational response than on the torsional response. Stagger angle variation has a greater effect on the torsional response than on the translational one. Also, variations in stagger angle have a much greater effect on the response amplitudes, both torsional and translational, than do variations in solidity. It should be noted that the design trend for modern compressors includes increased solidity and

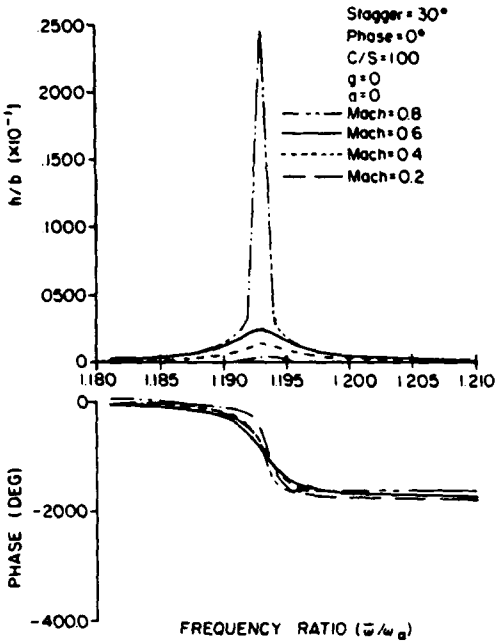

Fig. 12 Inlet Mach number effect on the coupled translational response.

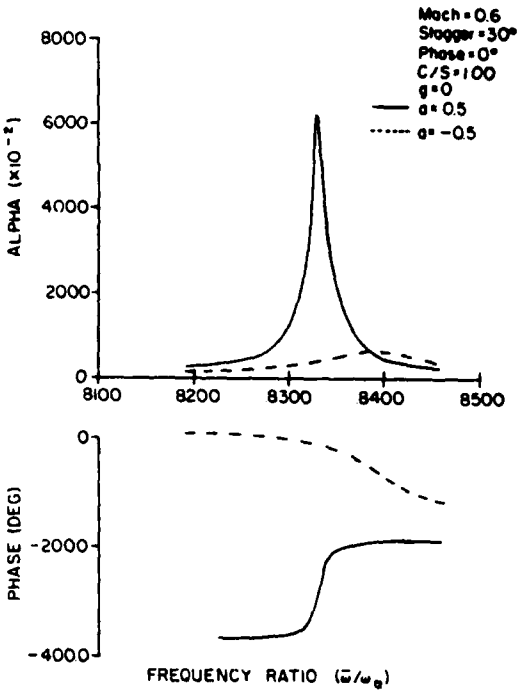

Fig. 13 Effect of elastic axis location on the coupled torsional response for (ω/ω_α) near ω_α.

stagger angle values. Hence, these results indicate that increased forced response problems, primarily associated with increased stagger angles, might be anticipated.

Figures 9 and 10 show the effect of interblade phase angle on the coupled airfoil forced response characteristics. The effect of variations in this parameter on the coupled torsional forced response are quite different than on the coupled translational response. For the torsion mode, there is only an extreme maximum response amplitude for a 0-deg interblade phase angle value. For all other values considered, the response amplitude curves are relatively flat and decreased from the 0 deg case by approximately 75 to 85%. The coupled translational response amplitudes all exhibit an extreme maximum response amplitude, i.e. none of the amplitude response curves are relatively flat. Also, although an interblade phase angle value of 0 deg results in the maximum forced translational response amplitude, varying the interblade phase angle away from 0 deg results in noticably smaller decreases in this maximum amplitude than were noted for the forced torsional response. In particular, for both the torsional and the translational cases, the largest decrease in the maximum response amplitude is associated with changing the interblade phase angle value from 0 to −90 deg. However, the maximum forced translational response decreased only 45%, whereas the corresponding forced torsional response decreased by 85%. In addition, since the smallest coupled torsional and translational response amplitudes correspond to negative interblade phase angle values (−90 deg in particular), then this would appear to be a desirable forced response design condition. In terms of the rotor-stator interaction forced response problem, a negative interblade phase angle value corresponds to a backward traveling wave as viewed from the stator vane frame of reference and arises when the number of rotor blades is greater than the number of stator vanes.

The effect of the inlet flow Mach number on the coupled torsional and translational forced response characteristics of the representative airfoil is demonstrated in Figs. 11 and 12, respectively. Increasing the Mach number, which also corresponds to decreasing the reduced frequency for a specific

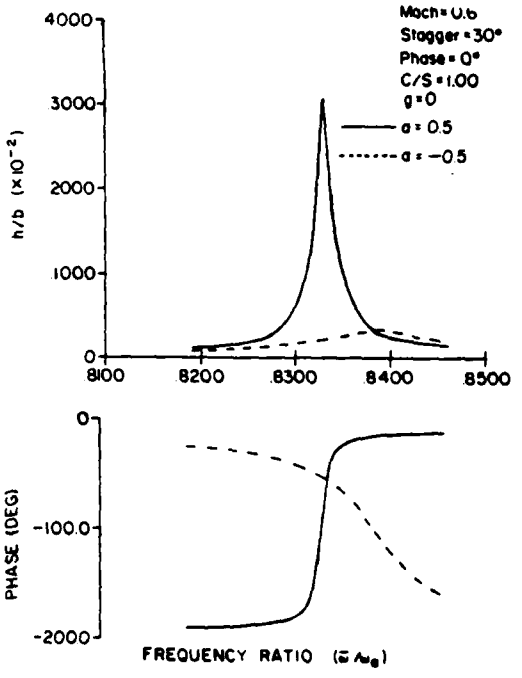

Fig. 14 Effect of elastic axis location on the coupled translational response for (ω/ω_α) near ω_α.

gust disturbance, increases both the coupled torsional and translational responses with a very dramatic increase associated with an increase in Mach number from 0.6 to 0.8. Also, for Mach numbers of 0.6 and smaller, the increase in the maximum response amplitude is much larger for the torsional mode than for the translational mode. In addition, the forcing

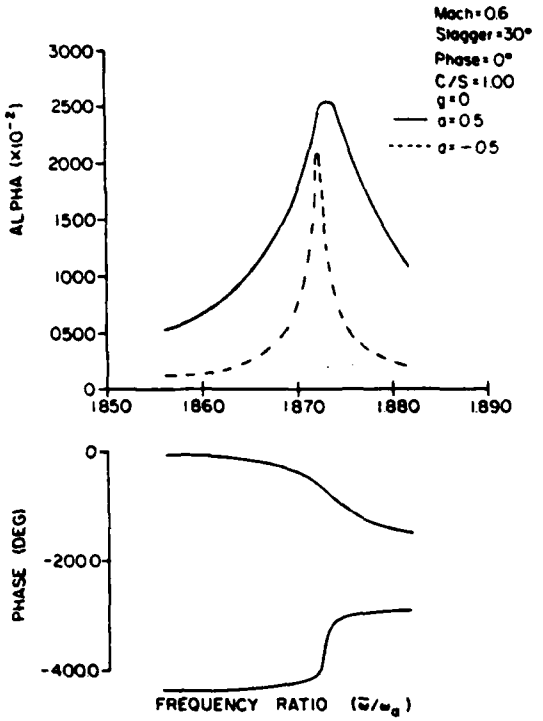

Fig. 15 Effect of elastic axis location on the coupled torsional response for $(\bar{\omega}/\omega_\alpha)$ near ω_h.

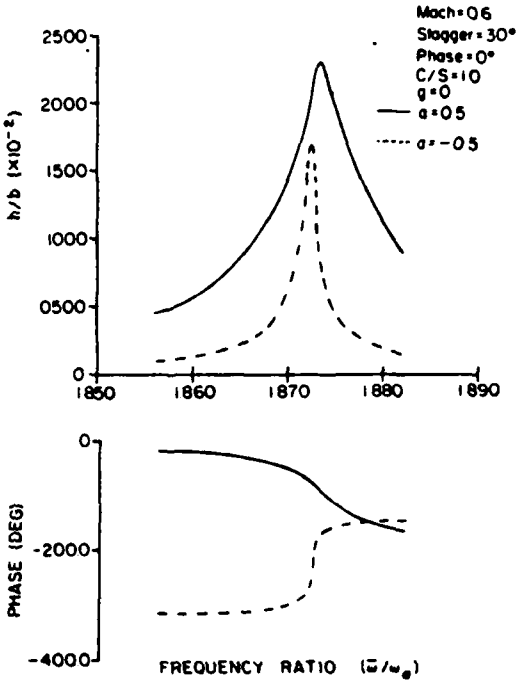

Fig. 16 Effect of elastic axis location on the coupled translational response for $(\bar{\omega}/\omega_\alpha)$ near ω_h.

function frequency at which the maximum amplitude response occurs is highly dependent on the Mach number for the torsional response, but is almost independent of this forcing frequency for the translational response case.

The effect of moving the elastic axis location to the ¼-chord and the ¼-chord locations on the coupled forced response of the representative airfoil is presented in Figs. 13 through 16. These results indicate that not only the response amplitude but also the forcing function frequency at which the maximum amplitude response occurs is strongly dependent on the position of the elastic axis. The maximum torsion and translation response amplitudes are found with the elastic axis at the ¼-chord location. Shifting the elastic axis forward to the ¼-chord location results in significantly decreasing both the torsional and translational response amplitudes near the airfoil torsional natural frequency, but only slightly decreasing these response amplitudes near the airfoil translational natural frequency. Also, shifting the elastic axis location aft from mid-chord to ¼-chord has the result of making the translational response in the neighborhood of the natural torsional frequency ($\bar{\omega}/\omega_\alpha \approx 1.0$) the same order of magnitude as the torsional response amplitude, indicating the significant additional coupling that arises when the elastic axis and the airfoil center of gravity do not coincide. Similar results are noted when the forcing function frequency is close to the natural translational frequency.

To demonstrate the interaction of two very closely-spaced torsional and translation modes, the bending stiffness of the representative airfoil was altered to make the ratio of translation to torsion natural frequencies 1.02. The variation with interblade phase angle values of these closely coupled forced torsional and translational responses was then investigated. The results are presented in Figs. 17 and 18. The coupled torsional response results (Fig. 17) show that, at a frequency ratio of 0.990, the response decreases as the interblade phase angle is varied from 0 to +90, −90, and 180 deg. At a frequency ratio of 1.015 the response increases by up to 65%.

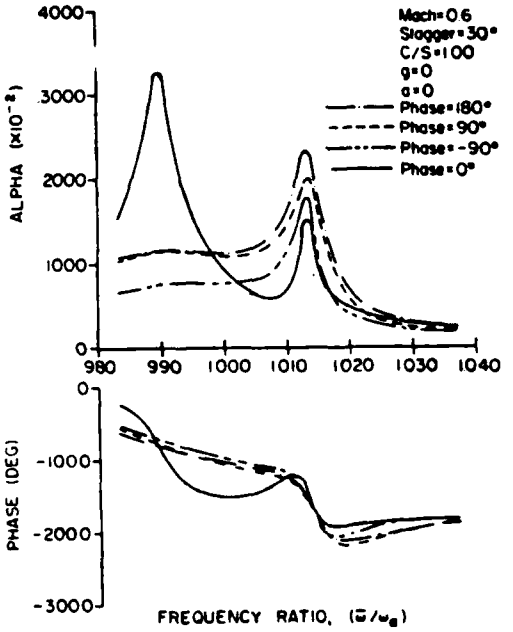

Fig. 17 Interblade phase angle effect on the coupled torsional response for nearly equal natural frequencies.

Figure 18 presents the variation of the forced translational response with the interblade phase angle as the parameter. In contrast to the torsional response results, minimal translational response is noted when the forcing function frequency is near the airfoil natural torsional frequency. However, when the forcing function frequency is near the airfoil natural translational frequency ($\bar{\omega}/\omega_\alpha \approx 1.015$), the

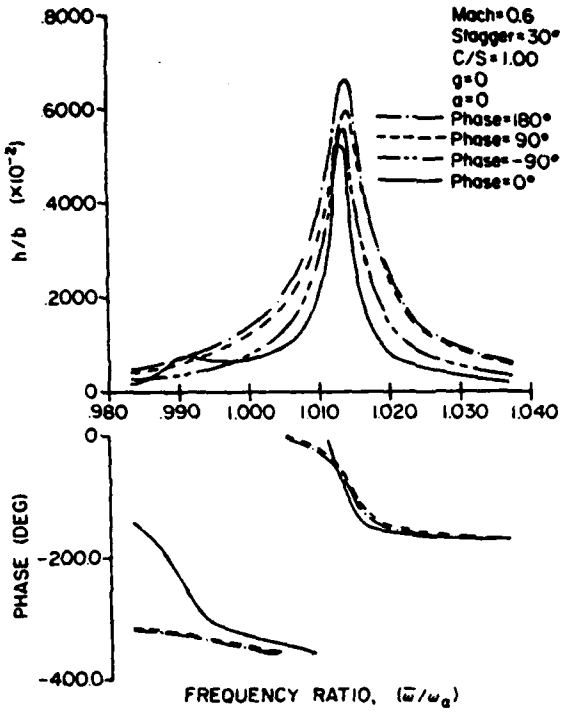

Fig. 18 Interblade phase angle effect on the coupled translational response for nearly equal natural frequencies.

forced translational amplitude is significant and increases as the interblade phase angle value is varied from 0 to 180 deg. A comparison of Figs. 17 and 18 at a frequency ratio close to 1.015 reveals a correspondence between the forced torsional response and the translational one. This is caused by the high degree of coupling that exists between the translational and torsional modes for the altered airfoil.

Summary and Conclusions

In this investigation, the coupled structural dynamic airfoil system forced response was determined utilizing an energy balance technique. The energy input to the system per cycle of oscillation was generated by the gust and, under certain conditions, the self-induced aerodynamic forces and moments. The energy dissipation per cycle of oscillation was associated with system structural damping, under some conditions the self-induced aerodynamic forces and moments, and the static moment term S_{α}. It should be noted that, for the uncoupled single-degree-of-freedom case, the dissipative coupling mechanism, S_{α}, is not considered.

The effects of the various aerodynamic parameters on the coupled translational and torsional mode forced response of a representative airfoil were then considered. The study showed the increased coupling between the torsion and translation modes as the corresponding undamped natural frequencies approach one another. It was also demonstrated that the coupled torsional and translational forced response amplitudes of a representative airfoil increased with: 1) decreased structural damping, 2) increased solidity values, 3) increased stagger angles, 4) increased inlet flow Mach numbers, 5) interblade phase angle values corresponding to forward traveling waves for the rotor-stator interaction case, and 6) shifting of the elastic axis location aft.

It should be noted that variations in the above parameters did not affect the magnitude of the resulting forced response equally nor did they always have equivalent effects on the torsional and translational response modes. For example, increasing the stagger angle and shifting the elastic axis aft resulted in significantly larger increases in all of the response amplitudes than did increasing the solidity. Also, the interblade phase angle, for example, had a much greater effect on the coupled torsion mode responses than on the translational ones. In addition, the forcing function frequencies at which the maximum torsional and translational responses occurred did not generally correspond to the airfoil natural torsional or tanslational frequencies. This was because the self-induced aerodynamic forces and moments result in an aerodynamic damping effect analogous to structural damping.

Acknowledgment

The Air Force Office of Scientific Research and Capt. Michael Francis, who served as the project's technical monitor, are gratefuly acknowledged for their support.

References

[1] "The Aerothermodynamics of Aircraft Gas Turbine Engines," AFAPL-TR 78-52, July 1978.

[2] Fleeter, S., Jay, R.L., and Bennett, W.A., "Rotor Wake Generated Unsteady Aerodynamic Response of a Compressor Stator," *ASME Journal of Engineering for Power*, Vol. 100, No. 4, Oct. 1978, pp. 664-675.

[3] Fleeter, S., "Aeroelasticity Research for Turbomachine Application," *Journal of Aircraft*, Vol. 16, May 1979, pp. 320-326.

[4] Platzer, M.F., "Unsteady Flows in Turbomachines—A Review of Recent Developments," AGARD-CP-227, Sept. 1977.

[5] Fung, Y.C., *An Introduction to the Theory of Aeroelasticity*, Dover Publications, New York, N.Y., 1969.

[6] Hoyniak, D. and Fleeter, S., "Prediction of Aerodynamically Induced Vibrations in Turbomachinery Blading," ASME Symposium in Fluid/Structure Interaction in Turbomachinery, Nov. 1981.

[7] Fleeter, S., "The Fluctuating Lift and Moment Coefficients for Cascaded Airfoils in a Nonuniform Compressible Flow," *Journal of Aircraft*, Vol. 10, Feb. 1973, pp. 93-98.

END

FILMED

2-86

DTIC